

Shape constrained kernel-weighted least squares: Estimating production functions for Chilean manufacturing industries

Daisuke Yagi¹, Yining Chen², Andrew L. Johnson^{1,3} and Timo Kuosmanen⁴

¹Texas A&M University

²London School of Economics and Political Science

³Osaka University

⁴Aalto University

November 12, 2018

Abstract

Two common approaches to nonparametric regression include local averaging and shape constrained regression. In this paper we examine a novel way to impose shape constraints on a local polynomial kernel estimator. The proposed approach is referred to as Shape Constrained Kernel-weighted Least Squares (SCKLS). Under regularity conditions, we prove the uniform consistency of SCKLS with the monotonicity and convexity/concavity constraints and establish its convergence rate. We also show that SCKLS is a generalization of Convex Nonparametric Least Squares (CNLS). In addition, we propose tests to validate whether shape constraints are correctly specified or not, and to check whether a function is affine. The competitiveness of SCKLS is shown in a comprehensive simulation study. Finally, we analyze Chilean manufacturing data using the SCKLS estimator and quantify production in the plastics and wood industries. Importantly we find firms that export have significantly higher productivity.

Keywords: Kernel Estimation, Multivariate Convex Regression, Nonparametric regression, Shape Constraints.

1 Introduction

Nonparametric methods avoid functional form misspecification, but may suffer from the curse of dimensionality. For modeling production with a production or a cost function, the flexible nature of nonparametric methods often cause difficulties in interpreting the results. However, microeconomic theory provides additional structure for modeling production which can be stated as shape constraints. Recently several nonparametric shape constrained estimators have been proposed that combine the advantage of avoiding parametric functional specification with improved small sample performance relative to unconstrained nonparametric estimators. Nevertheless, the existing methods have limitations regarding either estimation performance or computational feasibility, discussed in detail in Section 2. In this paper, we propose an estimator that imposes shape restrictions (focusing on concavity and monotonicity restrictions) on local kernel weighting methods. By combining local averaging with shape-constrained estimation, we hope to improve small sample performance by avoid overfitting.

Work on shape-constrained regression first started in the 1950s by Hildreth (1954), who studied the univariate regressor case with a least squares objective subject to monotonicity and concavity/convexity constraints. See also Brunk (1955) and Grenander (1956) for alternative shape constrained estimators. Under the concavity/convexity constraint, properties such as consistency, rate of convergence, and asymptotic distribution are shown by Hanson and Pledger (1976), Mammen (1991), and Groeneboom et al. (2001), respectively. In the multivariate case, consistency of the least squares estimator is shown by Seijo and Sen (2011) and Lim and Glynn (2012). Furthermore, when combining concavity/convexity with a monotonicity constraint, Kuosmanen (2008) investigated the characterization of the corresponding least squares estimator, which we will refer to as Convex Nonparametric Least Squares (CNLS) throughout this paper.

Regarding the nonparametric estimation implemented using kernel based methods, Birke and Dette (2007), Carroll et al. (2011), and Hall and Huang (2001) investigated the univariate case and proposed smooth estimators that can impose derivative-based constraints including monotonicity and concavity/convexity. Du et al. (2013) proposed Constrained Weighted Bootstrap (CWB) by generalizing Hall and Huang's method to the

multivariate regression setting. However, CWB still faces significant computational difficulties with global concave/convex constraint. Finally, we mention the work of Li et al. (2016), which extended Hall and Huang’s method to use the k -nearest neighbor approach subject to the monotonicity constraint.

In this paper, we propose a novel method called *Shape Constrained Kernel-weighted Least Squares* (SCKLS), which optimizes a local polynomial kernel criterion while estimating a multivariate regression function with shape constraints. Under the monotonicity and convex/concavity constraints, we prove uniform consistency and establish convergence rate of the SCKLS estimator. Furthermore, we show that the CNLS estimator can be viewed as a special case of the SCKLS estimator when the bandwidth of the kernel approaches zero. Kuosmanen (2008), Seijo and Sen (2011) and Lim and Glynn (2012) emphasize the potential advantage that CNLS does not have any tuning parameters to choose. Our proposed SCKLS estimator sheds further light on this issue: in the SCKLS framework, CNLS can be seen as the zero bandwidth estimator; we argue that, compared to unrestricted kernel methods, the SCKLS estimator is relatively robust to the bandwidth selected and is able to alleviate the well-known issues such as boundary inconsistency faced by the CNLS estimator.

Note that with n observations, CNLS impose $O(n^2)$ concavity/convexity constraints, which could lead to computational difficulties. Here we implement an iterative algorithm that reduce the number of constraints building on the ideas in Lee et al. (2013) and estimate the function on a grid. We then validate the performance of the SCKLS estimator via Monte Carlo simulations. For a variety of parameter settings we find the performance of SCKLS to be better or at least competitive with the CNLS and the CWB estimators. We also investigate the use of variable bandwidth methods¹ and propose practical ways to further improve the performance of SCKLS.

Crucially, we also propose a hypothesis test to validate the shape constraints imposed. Having a test that validates the shape constraints is critical because otherwise our estimation procedure would have contain bias under misspecified shape restrictions. Furthermore, motivated by Sen and Meyer (2017), we show how to use the SCKLS estimator to test affin-

¹A variable bandwidth method allows the bandwidth associated with a particular regressor to vary with the density of the data.

ity. Again, the usefulness and effectiveness of these two tests are demonstrated through both theory and Monte Carlo simulations.

Finally, we apply the SCKLS estimator empirically on Chilean manufacturing data from the Chilean Annual Industrial Survey. The estimation results provide a concise description of the supply-side of the Chilean plastic and wood industry as we report marginal productivity, marginal rate of substitution and most productive scale size. The impact of exporting on productivity are also investigated by including additional predictors of output in a semi-parametric model. We find that exporting is correlated with higher productivity supporting international trade theories that argue high productivity firms are more likely to compete in international markets.

This paper focuses on production functions. This aim guides the selection of the polynomial function used in estimation, the data generation processes (DGP) in the Monte Carlo simulations, and for the application analyzing the Chilean manufacturing data, and thus, the primary shape constraints of interest here are monotonicity and concavity. These assumptions are motivated from standard economic theory for production functions and consumer preferences (Varian, 1982, 1984). However, the methods proposed in the paper are general and applicable for other applications of shape restricted functional estimation, as discussed in section 3.2.

The remainder of this paper is as follows. Section 2 describes the model and the existing estimators, CNLS and CWB. Section 3 presented the proposed estimator, SCKLS. Section 4 contains the statistical properties of SCKLS estimator, while Section 5 discusses a test for concavity and monotonicity, and how SCKLS can be used to test whether a function is affine. Monte Carlo simulation results for a set of three estimator (SCKLS, CNLS and CWB) under several different experimental settings are shown in Section 6. Section 7 applies the SCKLS estimator to estimate a production function for both the Chilean plastics and wood industries. Section 8 concludes and suggests future research directions. An appendix discusses several extensions to the CWB estimator and describes the relationship between SCKLS, CWB and CNLS. A more extensive set of simulation results are reported and details of the iterative algorithm for SCKLS are also provided.

2 Model Framework and Existing Estimators

The following section introduces the model framework and describes two existing nonparametric estimation methods with concavity/convexity and monotonicity constraints.

2.1 Model

Suppose we observe n pairs of input and output data, $\{\mathbf{X}_j, y_j\}_{j=1}^n$, where for every $j = 1, \dots, n$, $\mathbf{X}_j = (X_{j1}, \dots, X_{jd})' \in \mathbb{R}^d$ is a d -dimensional input vector, and $y_j \in \mathbb{R}$ is an output scalar. Consider the following regression model

$$y_j = g_0(\mathbf{X}_j) + \epsilon_j, \quad \text{for } j = 1, \dots, n,$$

where ϵ_j is a random variable satisfying $E(\epsilon_j | \mathbf{X}_j) = 0$. The regression function $g_0 : \mathbb{R}^d \rightarrow \mathbb{R}$ is assumed to belong to a class of functions, G , that satisfies certain shape restrictions. Building on the structure proposed by Du et al. (2013), our estimator can impose any shape restriction that can be modelled as a lower or upper bound on a derivative. Examples are supermodularity, convexity, monotonicity, or quasi-convexity. Section 3.2 discusses the most general setting. For purposes of concreteness, and in view of the application to production functions, we will focus on imposing monotonicity and global convexity/concavity. Specifically, g_0 is concave if:

$$\lambda g_0(\mathbf{x}_1) + (1 - \lambda)g_0(\mathbf{x}_2) \leq g_0(\lambda \mathbf{x}_1 + (1 - \lambda)\mathbf{x}_2), \quad \forall \mathbf{x}_1, \mathbf{x}_2 \in \mathbb{R}^d \text{ and } \forall \lambda \in [0, 1]$$

Furthermore, saying g_0 is monotonically increasing means that

$$\text{if } \mathbf{x}_1 \leq \mathbf{x}_2, \text{ then } g_0(\mathbf{x}_1) \leq g_0(\mathbf{x}_2),$$

where the inequality of $\mathbf{x}_1 \leq \mathbf{x}_2$ means that every component of \mathbf{x}_2 is greater than or equal to the corresponding component of \mathbf{x}_1 .

2.2 Some related work

2.2.1 Convex Nonparametric Least Squares (CNLS)

Kuosmanen (2008) extends Hildreth’s least squares approach to the multivariate setting with a multivariate input, and coins the term “Convex Nonparametric Least Squares” (CNLS)². CNLS builds upon the assumption that the true but unknown production function g_0 belongs to the class of continuous, monotonic increasing and globally concave functions, denoted by G_2 in this paper. Given the observations $\{\mathbf{X}_j, y_j\}_{j=1}^n$, a set of unique fitted values, $\hat{y}_j = \hat{\alpha}_j + \hat{\beta}_j' \mathbf{X}_j$, can be found by solving the quadratic programming (QP) problem

$$\begin{aligned} \min_{\alpha, \beta} \quad & \sum_{j=1}^n (y_j - (\alpha_j + \beta_j' \mathbf{X}_j))^2 \\ \text{subject to} \quad & \alpha_j + \beta_j' \mathbf{X}_j \leq \alpha_l + \beta_l' \mathbf{X}_j, \quad j, l = 1, \dots, n \\ & \beta_j \geq 0, \quad j = 1, \dots, n \end{aligned} \tag{1}$$

where α_j and β_j define the intercept and slope parameters that characterize the estimated set of hyperplanes. The inequality constraints in (1) can be interpreted as a system of Afriat inequalities (Afriat, 1972; Varian, 1984) to impose concavity constraints. We emphasize that CNLS does not assume or restrict the domain G_2 to only include the piece-wise affine function. We also note that the functional estimates resulting from (1) is unique only at the observed data points. Though the resulting estimate from (1) is typically piece-wise affine, we note that piece-wise affine function can be used to approximate functions of many different forms. In addition, when $d = 1$, Chen and Wellner (2016) and Ghosal and Sen (2016) proved that the CNLS-type estimator attains $n^{-1/2}$ pointwise rate of convergence if the true function is piece-wise linear.

Finally, we remark that CNLS is related to the method of sieves (Grenander, 1981; Chen and Qiu, 2016). The estimator could be rewritten as

$$\hat{g}_n \in \operatorname{argmin}_{g \in \mathcal{G}^n} \frac{1}{n} \sum_{j=1}^n (y_j - g(\mathbf{X}_j))^2,$$

²A related maximum likelihood formulation was proposed by Banker and Maindiratta (1992), with its consistency proved by Sarath and Maindiratta (1997).

where $\mathcal{G}^n = \{g : \mathbb{R}^d \rightarrow \mathbb{R} \mid g(\mathbf{x}) = \min_{j \in \{1, \dots, n\}} (\alpha_j + \beta_j' \mathbf{x}), \text{ with } \beta_j \geq 0 \text{ for } j = 1, \dots, n\}$. However, since the sets $\mathcal{G}^1, \mathcal{G}^2, \dots$ are not compact, most known results on sieves do not directly apply here.

2.2.2 Constrained Weighted Bootstrap (CWB)

Hall and Huang (2001) proposed the monotone kernel regression method in univariate function. Du et al. (2013) generalized this model to handle multiple general shape constraints for multivariate functions, which they refer to as Constrained Weighted Bootstrap (CWB). CWB estimator is constructed by introducing weights for each observed data point. The weights are selected to minimize the distance to unconstrained estimator while satisfying the shape constraints. The function is estimated as

$$\hat{g}(\mathbf{x}|\mathbf{p}) = \sum_{j=1}^n p_j A_j(\mathbf{x}) y_j \quad (2)$$

where $\mathbf{p} = (p_1, \dots, p_n)'$, p_j is the weights introduced for each observation and $A_j(\mathbf{x})$ is a local weighting matrix (e.g. local linear kernel weighting matrix). Du et al. (2013) relaxed the restriction imposed by Hall and Huang (2001) that p_j is non-negative and propose to calculate p_j by minimizing the distance to unrestricted weights, $p_u = 1/n$, under derivative-based shape constraints³. The problem is formulated as follows.

$$\begin{aligned} \min_{\mathbf{p}} \quad & D(\mathbf{p}) = \sum_{j=1}^n (p_j - p_u)^2 = \sum_{j=1}^n (p_j - 1/n)^2 \\ \text{subject to} \quad & l(\mathbf{x}_i) \leq \hat{g}^{(\mathbf{s})}(\mathbf{x}_i|\mathbf{p}) \leq u(\mathbf{x}_i), \quad i = 1, \dots, m \end{aligned} \quad (3)$$

where \mathbf{x}_i represents a set of points for evaluating constraints, the elements of \mathbf{s} represent the order of partial derivative, and $g^{\mathbf{s}}(\mathbf{x}) = [\partial^{s_1} g(\mathbf{x}) \cdots \partial^{s_r} g(\mathbf{x})] / [\partial x_1^{s_1} \cdots \partial x_r^{s_r}]$ for $\mathbf{s} = (s_1, s_2, \dots, s_r)$. Here the shape restrictions (e.g. concavity/convexity and monotonicity constraints) are imposed at a set of evaluation points $\{\mathbf{x}_i\}_{i=1}^m$ through setting appropriate lower and upper bounds to the corresponding partial derivatives of the function. Although

³The use of the equality constraint $\sum_j p_j = 1$ in Du et al. (2013) is a typo, and this condition is not used by them. In fact, it may harm the estimation procedure. Our empirical results show that this equality constraint only makes difference in very few cases and the difference is typically small.

CWB results in a smooth function, the estimated function only satisfies the shape restrictions locally around the evaluation points on which they are imposed. One way to interpret the CWB estimator is as a two-step process: 1) estimate an unconstrained kernel estimator; 2) find the shape constrained function that is as close as possible (as measured by the Euclidean distance in p -space) to the unconstrained kernel estimator. Though conceptually simple, this procedure could potentially pull the functional estimate away from the true function since the unconstrained kernel is very sensitive to the bandwidth choice (DiNardo and Tobias, 2001). On the one hand, if the bandwidth is too small, the unconstrained kernel estimator under-smoothes and very sensitive to the observations, and thus, it could be pulled away from the true function. On the other hand, if the bandwidth is too large, then the unconstrained estimator over-smoothes, and thus, it is also pulled away from the true function. Consequently, the CWB estimator tends to suffer from computational difficulties and occasionally poor estimates in small samples, as demonstrated in Section 6. In Appendix A.2, we suggest changing the objective function to minimize the distance from the estimated function to the observed data, which seems to improve the estimates⁴.

3 Shape Constrained Kernel-weighted Least Squares (SCKLS)

This section explains the proposed estimation method based on the Local Linear and Local Polynomial estimators.

3.1 SCKLS with Local Linear

Given the n pairs of observations, $\{\mathbf{X}_j, y_j\}_{j=1}^n$, the (multivariate) local linear kernel estimator developed by Stone (1977) and Cleveland (1979) is defined as

$$\min_{a, \mathbf{b}} \sum_{j=1}^n (y_j - a - (\mathbf{X}_j - \mathbf{x})' \mathbf{b})^2 K \left(\frac{\mathbf{X}_j - \mathbf{x}}{\mathbf{h}} \right) \quad (4)$$

⁴We refer to the estimator that minimizes the distance from the estimated function to the observed data as the CWB in y -space, and to the original CWB estimator as CWB in p -space, respectively. This estimator is also proposed in Li et al. (2016). Appendix E.1 presents a comparison of these estimators.

where a is a functional estimate, and \mathbf{b} is an estimate of the slope of the function at \mathbf{x} with \mathbf{x} being an arbitrary point in the input space, $K\left(\frac{\mathbf{X}_j - \mathbf{x}}{\mathbf{h}}\right)$ denotes a product kernel, and \mathbf{h} is a vector of the bandwidth (see Racine and Li (2004) for more detail). The objective function uses kernel weights, so more weight is given to the observations that are closer to the point \mathbf{x} .

We introduce a set of m points, $\mathbf{x}_1, \dots, \mathbf{x}_m$, for evaluating constraints, which we call evaluation points, and impose shape constraints on the local linear kernel estimator. In the spirit of local linear kernel estimator, we define Shape Constrained Kernel-weighted Least Squares (SCKLS) estimator as

$$\begin{aligned} \min_{a_i, \mathbf{b}_i} \quad & \sum_{i=1}^m \sum_{j=1}^n (y_j - a_i - (\mathbf{X}_j - \mathbf{x}_i)' \mathbf{b}_i)^2 K\left(\frac{\mathbf{X}_j - \mathbf{x}_i}{\mathbf{h}}\right) \\ \text{subject to} \quad & l(\mathbf{x}_i) \leq \hat{g}^{(s)}(\mathbf{x}_i | \mathbf{a}, \mathbf{b}) \leq u(\mathbf{x}_i), \quad i = 1, \dots, m \end{aligned} \quad (5)$$

where $\mathbf{a} = (a_1, \dots, a_m)'$ and $\mathbf{b} = (\mathbf{b}'_1, \dots, \mathbf{b}'_m)'$. For the case of monotonicity and concavity, these constraints can be written explicitly as

$$\begin{aligned} \min_{a_i, \mathbf{b}_i} \quad & \sum_{i=1}^m \sum_{j=1}^n (y_j - a_i - (\mathbf{X}_j - \mathbf{x}_i)' \mathbf{b}_i)^2 K\left(\frac{\mathbf{X}_j - \mathbf{x}_i}{\mathbf{h}}\right) \\ \text{subject to} \quad & a_i - a_l \geq \mathbf{b}'_i(\mathbf{x}_i - \mathbf{x}_l), \quad i, l = 1, \dots, m \\ & \mathbf{b}_i \geq 0, \quad i = 1, \dots, m \end{aligned} \quad (6)$$

The first set of constraints in (6) imposes concavity and the second set of constraints imposes non-negativity of \mathbf{b}_i at each evaluation point \mathbf{x}_i . From the results of (6), we can then define the SCKLS estimator to be the function $\hat{g}_n : \mathbb{R}^d \rightarrow \mathbb{R}$ such that

$$\hat{g}_n(\mathbf{x}; \hat{\mathbf{a}}, \hat{\mathbf{b}}) = \min_{i \in \{1, \dots, m\}} \left\{ \hat{a}_i + (\mathbf{x} - \mathbf{x}_i)' \hat{\mathbf{b}}_i \right\} \quad (7)$$

for any $\mathbf{x} \in \mathbb{R}^d$, where \hat{a}_i and $\hat{\mathbf{b}}_i$ are the solutions of (6). Note that (7) implies the functional estimate is constructed by linear interpolation between the evaluation points rather than reweighting the unrestricted kernel. This differentiates SCKLS from CWB and assures the estimated function is globally concave.

A standard method for determining the evaluation points \mathbf{x}_i is to construct a uniform grid. As the density of \mathbf{x}_i increases, the estimated function potentially has more hyperplane components and is more flexible; however, the computation time typically increases. If a smooth functional estimate is preferred, see Nesterov (2005) and Mazumder et al. (2015), where methods for smoothing are provided⁵.

Figure 1 is meant to be illustrative of the relationship between the SCKLS, CNLS and CWB estimators in a two-dimensional estimated ϵ -space where there are more than two observations, but for the rest of the $n - 2$ observations, their estimated ϵ_j s are held fix. The gray area indicates the cone of concave and monotonic functions. CNLS estimates a monotonic and concave function while minimizing the sum of squared errors, that is, minimizing the distance from the origin to the cone in the estimated ϵ -space. CWB estimates a monotonic and concave function by finding the closest point, measured in p -space, on the cone of concave and monotonic functions to unconstrained kernel estimate. SCKLS minimizes a weighted function of estimated errors, and therefore avoids overfitting the observed data, but also attempts to fit the data as closely as possible, rather than minimizing the distance from the unconstrained kernel estimator.

Our primary application of interest is production functions estimated for census manufacturing data where the input distributions are often highly skewed meaning there are many small establishments, but relatively few large establishments⁶. Below we propose two methods to address this issue.

First, we propose to use a k -nearest neighbor (k -NN) approach in SCKLS which we will refer to as SCKLS k -NN which is in spirit similar to the extension to the CWB-type estimator proposed by Li et al. (2016). The k -NN approach uses a smaller bandwidth for smoothing in dense data regions and a larger bandwidth when the data is sparse. For a further description of the method, see for example Li and Racine (2007). The formulation of SCKLS k -NN leads to a different weighting in the objective function, as illustrated in the following.

⁵Appendix B presents a limited comparison between shape constrained B-splines and SCKLS. The results indicate that, even with the smooth B-splines estimator, the estimated function is often approximately piece-wise linear when the true function is monotonic and concave and the estimator is fit using a small set of data.

⁶An establishment is defined as a single physical location where business is conducted or where services or industrial operations are performed.

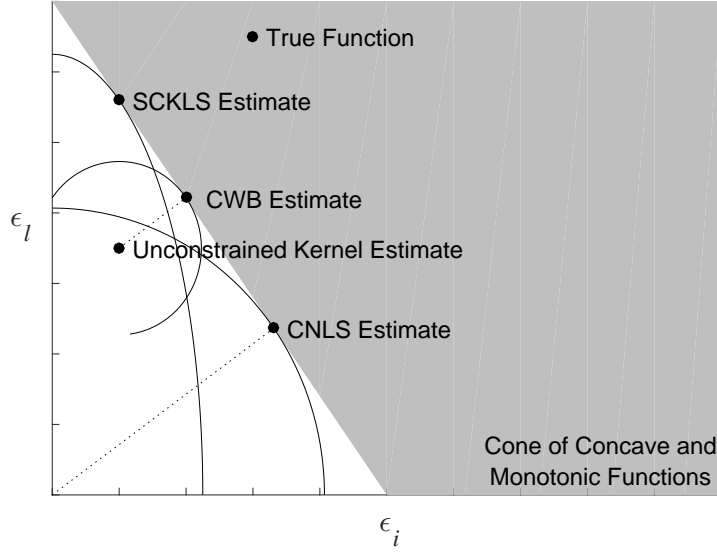


Figure 1. Comparison of different estimators in the estimated- ϵ -space.

$$\begin{aligned}
 \min_{a_i, \mathbf{b}_i} \quad & \sum_{i=1}^m \sum_{j=1}^n (y_j - a_i - (\mathbf{X}_j - \mathbf{x}_i)' \mathbf{b}_i)^2 w \left(\frac{\|\mathbf{X}_j - \mathbf{x}_i\|}{R_{\mathbf{x}_i}} \right) \\
 \text{subject to} \quad & a_i - a_l \geq \mathbf{b}_i' (\mathbf{x}_i - \mathbf{x}_l), \quad i, l = 1, \dots, m \\
 & \mathbf{b}_i \geq 0, \quad i = 1, \dots, m
 \end{aligned} \tag{8}$$

where $w(\cdot)$ is a general weight function, $\|\cdot\|$ is the Euclidian norm and $R_{\mathbf{x}_i}$ denotes the Euclidian distance between \mathbf{x}_i and k -th nearest neighbor of \mathbf{x}_i among the set of all covariates $\{\mathbf{X}_j\}_{j=1}^n$.

Alternatively, we note that for CWB and SCKLS estimators one needs to specify how to select the evaluation points before implementation. As mentioned before, the standard method is to use a uniform grid where each dimension is divided into equal spaces. However, we can also address the input skewness issue by constructing the evaluation points differently, using a non-uniform grid method. To do so, we first use kernel density estimation to estimate the density function for each input dimension. Then we take the equally spaced percentiles of the estimated density function and construct non-uniform grid. Figure 2 demonstrates how the non-uniform grid are constructed for the 2-dimensional case.

In this example, we set the minimum and maximum of the observed inputs (with respect to each coordinate) as the edge of the grid, and compute equally spaced percentile. We discuss the impacts of these extensions in section 6 where the simulation results are presented.

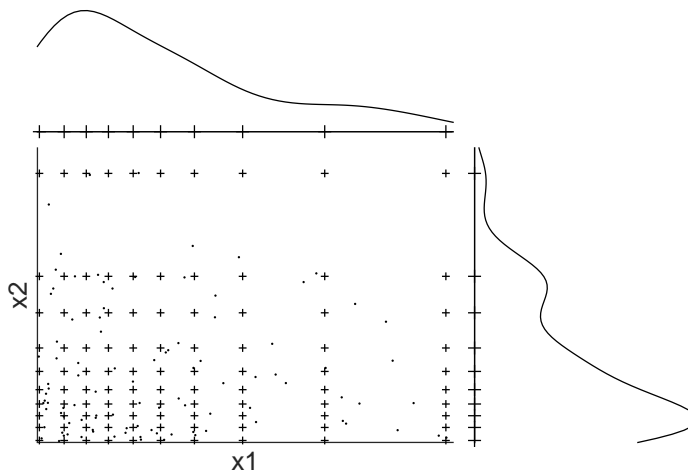


Figure 2. Example of non-uniform grid with kernel density estimation.

3.2 SCKLS with Local Polynomial

With the proposed estimator in (5), we are only able to impose the constraints by using the functional estimate and/or first partial derivatives. For constraints involving a higher order of derivatives, we need to formulate SCKLS estimator with a higher order local polynomial function. For the multivariate local polynomial, we borrow the following notation from Masry (1996).

$$\begin{aligned}
 \mathbf{r} &= (r_1, \dots, r_d), & \mathbf{r}! &= r_1! \times \dots \times r_d!, & \bar{\mathbf{r}} &= \sum_{k=1}^d r_k, \\
 \mathbf{x}^{\mathbf{r}} &= x_1^{r_1} \times \dots \times x_d^{r_d}, & \sum_{0 \leq \bar{\mathbf{r}} \leq p} &= \sum_{k=0}^p \sum_{r_1=0}^k \dots \sum_{r_d=0}^k, & & \text{and} \\
 (D^{\mathbf{r}} g)(\mathbf{x}) &= \frac{\partial^{\mathbf{r}} g(\mathbf{x})}{\partial x_1^{r_1} \dots \partial x_d^{r_d}}
 \end{aligned}$$

With this notation, we can approximate any function $g : \mathbb{R}^d \rightarrow \mathbb{R}$ locally (around any \mathbf{x}) using a multivariate polynomial of total order p , given by

$$g(\mathbf{z}) := \sum_{0 \leq \bar{r} \leq p} \frac{1}{\mathbf{r}!} (D^{\bar{r}}) g(\mathbf{x}) (\mathbf{z} - \mathbf{x})^{\bar{r}}. \quad (9)$$

We now define the SCKLS estimator with a local polynomial function of order p as follows:

$$\begin{aligned} \min_{\mathbf{a}_i, \mathbf{b}_i} \quad & \sum_{i=1}^m \sum_{j=1}^n \left(y_j - \sum_{0 \leq \bar{r} \leq p} \mathbf{b}'_i (\mathbf{X}_j - \mathbf{x}_i)^{\bar{r}} \right)^2 K \left(\frac{\mathbf{X}_j - \mathbf{x}_i}{\mathbf{h}} \right) \\ \text{subject to} \quad & l(\mathbf{x}_i) \leq \hat{g}^{(s)}(\mathbf{x}_i | \mathbf{b}) \leq u(\mathbf{x}_i), \quad i = 1, \dots, m \end{aligned} \quad (10)$$

where \mathbf{b}_i is the functional or derivative estimates at each evaluation points and $\mathbf{b} = (\mathbf{b}'_1, \dots, \mathbf{b}'_m)'$. When we select $p = 1$, then the problem becomes exactly same as the proposed estimator of (5). This extension allows us to make the proposed methods more general and applicable for other applications of shape restricted functional estimation in which higher order derivative restricts may be required. From a computational complexity point of view, it is still optimizing a quadratic objective function within a convex solution space, and thus, the problem is still typically solvable within polynomial time.

As demonstrated in Li and Racine (2007), the rate of convergence of local polynomial estimator is the same for $p = 1$ and $p = 2$. One could attempt to select a polynomial estimator with $p \geq 3$ to improve its convergence performance (at least theoretical). But that would require much stronger assumption on the smoothness of g_0 , and would lead to additional computational burden⁷. Our experience suggests that SCKLS inherits these properties from the local polynomial method. Therefore, in practice, with only monotonicity and concavity/convexity constraints it suffices to consider SCKLS with $p = 1$ (i.e. local linear).

⁷While the optimization problem is still polynomial time solvable, the number of decision variables would increase and the constraint matrix would become significantly more dense, leading to computational challenges.

4 Properties of SCKLS

For mathematical concreteness, we next consider the statistical properties of SCKLS with local linear function under monotonicity and concavity constraints. We conjecture that results for other shape constraints can be derived in a similar fashion. First, we show the uniform consistency and the convergence rate of SCKLS. Second, we investigate the relationship between the SCKLS, CNLS, and sign constrained linear regression. Specifically, we show that (i) as the bandwidth in the SCKLS estimator approaches to zero, its estimate converges to the CNLS estimate; (ii) as the bandwidth in the SCKLS estimator approaches to infinity, its estimate converges to linear regression estimate subject to some sign constraints. Proofs of all the theorems are in Appendix C.

4.1 Uniform consistency and convergence rate of SCKLS

Recall that G_2 is the class of functions which are continuous, monotonically increasing and globally concave, and g_0 is the truth to be estimated from n pairs of observations. A set of assumptions are needed:

Assumption 1.

- (i) $\{\mathbf{X}_j, y_j\}_{j=1}^{\infty}$ be a sequence of i.i.d. random variables.
- (ii) $y_j = g_0(\mathbf{X}_j) + \epsilon_j$, with $\epsilon_j \stackrel{i.i.d.}{\sim} Z$ (independent of \mathbf{X}_j), $E(\epsilon_j) = 0$ and $E(\epsilon_j^4) < \infty$.
- (iii) $g_0 \in G_2$ and is twice-differentiable.
- (iv) \mathbf{X}_1 follows a distribution with continuous density function f and support \mathbf{S} . Here \mathbf{S} is a convex, non-degenerate and compact subset of \mathbb{R}^d . Moreover,

$$\min_{\mathbf{x} \in \mathbf{S}} f(\mathbf{x}) > 0.$$

- (v) $K(\cdot)$ is a bounded second order kernel with convex and compact support.
- (vi) For expositional simplicity, we set the bandwidth associated with each explanatory variable, h_k , for $k = 1, \dots, d$, to be $h_1 = \dots = h_d = h$ and satisfies $h = O(n^{-1/(4+d)})$ as $n \rightarrow \infty$.

Here (i) and (ii) state that the data is i.i.d. and the noise is also i.i.d. (iii) says that the constraints we impose on the SCKLS estimator are satisfied by the true function. (iv) makes further assumption on the distribution of the covariates. (v) is rather standard in local polynomial estimation to facilitate the theoretical analysis. Finally (vi) assures the bandwidths become sufficiently small as $n \rightarrow \infty$ so the bias from local averaging goes to zero. For details of the consistency of local linear estimator and a discussion of some of these conditions, see Masry (1996), Li and Racine (2007) and Fan and Guerre (2016).

Two different scenarios are considered, where we either fix the number of evaluation points (denoted by m), or let it grow with the number of observations n .

Assumption 2.

- (i) *The set of evaluation points $\{\mathbf{x}_1, \dots, \mathbf{x}_m\}$ is fixed, with each \mathbf{x}_i ($i = 1, \dots, m$) lying in the interior of \mathbf{S} (i.e. the support of the input, as defined in Assumption 1(iv)).*
- (ii) *The number of evaluation points m (as a function of n) $\rightarrow \infty$ as $n \rightarrow \infty$. Moreover, for simplicity, we assume that the empirical distribution of $\{\mathbf{x}_1, \dots, \mathbf{x}_m\}$ converges to a distribution Q that has support \mathbf{S} and a continuous density function $q : \mathbf{S} \rightarrow \mathbb{R}$ satisfying $\min_{\mathbf{x} \in \mathbf{S}} q(\mathbf{x}) > 0$.*

Theorem 1.

1. **(The case of a fixed m)** *Suppose that Assumption 1(i)-1(vi) and Assumption 2(i) hold. Then, as $n \rightarrow \infty$, with probability one, the estimates from SCKLS satisfy*

$$\hat{a}_i \rightarrow g_0(\mathbf{x}_i) \quad \text{and} \quad \hat{\mathbf{b}}_i \rightarrow \frac{\partial g_0}{\partial \mathbf{x}}(\mathbf{x}_i)$$

for all $i = 1, \dots, m$.

2. **(The case of an increasing m)** *Suppose that Assumption 1(i)-1(vi) and Assumption 2(ii) hold. Let \mathbf{C} be any fixed closed set that belongs to the interior of \mathbf{S} . Then with probability one, as $n \rightarrow \infty$, the SCKLS estimator satisfies*

$$\sup_{\mathbf{x} \in \mathbf{C}} |\hat{g}_n(\mathbf{x}) - g_0(\mathbf{x})| \rightarrow 0.$$

Theorem 2. *Suppose that Assumption 1(i)-1(vi) and Assumption 2(i) or 2(ii) hold. Then,*

$$\frac{1}{m} \sum_{i=1}^m \{\hat{g}_n(\mathbf{x}_i) - g_0(\mathbf{x}_i)\}^2 = O(n^{-4/(4+d)} \log n)$$

In the above, we only managed to show that the SCKLS estimator converges at the evaluation points or in the interior of the domain. It is known that shape-constrained estimators tend to suffer from bad boundary behaviours. However, if we let the number of evaluation points, m , grow at a rate slower than n , we can both alleviate the boundary inconsistency and improve the computational efficiency.

Assumption 3. *The number of evaluation points $m = O(n^{2/(4+d)} / \log n)$ as $n \rightarrow \infty$.*

Theorem 3. *Suppose that Assumption 1(i)-1(vi), Assumption 2(ii) and Assumption 3 hold. Then, with probability one, as $n \rightarrow \infty$, the SCKLS estimator satisfies*

$$\sup_{\mathbf{x} \in \mathcal{S}} |\hat{g}_n(\mathbf{x}) - g_0(\mathbf{x})| \rightarrow 0.$$

4.2 Special Cases of SCKLS

Let \hat{g}_n and \hat{g}_n^{CNLS} denote the SCKLS estimator and the CNLS estimator respectively. We will next examine the relationship between them.

Assumption 4. *The set of evaluation points is equal to the set of sample input vectors, i.e. $m = n$ and $\mathbf{x}_i = \mathbf{X}_i$ for $i = 1, \dots, n$.*

Theorem 4. *Suppose that Assumption 4 holds. Then, for any n , when the vector of bandwidth approaches zero, i.e. $\|\mathbf{h}\| \rightarrow \mathbf{0}$ (where $\mathbf{h} = (h_1, \dots, h_d)'$), the SCKLS estimator \hat{g}_n converges to the CNLS estimator \hat{g}_n^{CNLS} pointwise at $\mathbf{X}_1, \dots, \mathbf{X}_n$.*

Based on Theorem 4, the CNLS estimator could be viewed as a special case of the SCKLS estimator. Note that in comparison to the CNLS estimator, our SCKLS estimator has tuning parameters, which to some extent control the bias–variance tradeoff (in a non-trivial way given the shape restrictions). For reasonable values of these tuning parameters, the SCKLS estimator performs better than the CNLS, see Section 6. This is especially

true for the estimates close to the boundary of the input space, where imposing the shape constraint alone could lead to overfitting of the data, and thus biased estimates. Indeed, in view of Theorem 3, we can immediately derive that

$$E \sup_{\mathcal{S}} |\hat{g}_n(\mathbf{x}) - g_0(\mathbf{x})| < E \sup_{\mathcal{S}} |\hat{g}_n^{CNLS}(\mathbf{x}) - g_0(\mathbf{x})|.$$

for sufficiently large n .

Additional equivalence results can also be shown. Theorem 5 shows the equivalence of linear regression subject to monotonicity constraints and the SCKLS estimator when the bandwidth vector approaches infinity.

Theorem 5. *Given Assumption 1(v). For any given n , when the bandwidth vector approaches to infinity (i.e. $\min_{k=1,\dots,d} h_k \rightarrow \infty$), the SCKLS estimator converges to the least squares estimator of the linear regression model subject to monotonicity constraints.*

In practice, we could use leave-one-out cross-validation for the selection of the bandwidth vector \mathbf{h} . More details are mentioned in our simulation study in Section 6.

5 Hypothesis testing for shapes

5.1 Testing for monotonicity and concavity

So far we have assumed in our estimation procedures that $g_0 \in G_2$, where G_2 is the class of functions which are continuous, monotonically increasing and globally concave. Admittedly, our estimators would be inappropriate if these shape constraints are not fulfilled by g_0 . In the following, we propose a procedure based on the SCKLS estimators for testing

$$H_0 : \{g_0 : \mathcal{S} \rightarrow \mathbb{R}\} \in G_2 \quad \text{against} \quad H_1 : \{g_0 : \mathcal{S} \rightarrow \mathbb{R}\} \notin G_2.$$

Our testing procedure can be divided into three main steps:

1. Denote the set of evaluation points for SCKLS by $\{\mathbf{x}_1, \dots, \mathbf{x}_m\}$. Let \hat{g}_n be the SCKLS estimator based on $\{\mathbf{X}_j, y_j\}_{j=1}^n$ with the monotonicity and concavity constraints, and

let \tilde{g}_n be the corresponding local linear estimator without any shape constraint (but with the same bandwidth \mathbf{h}_n). The test statistics is defined as

$$T_n := \frac{1}{m} \sum_{i=1}^m \{\hat{g}_n(\mathbf{x}_i) - \tilde{g}_n(\mathbf{x}_i)\}^2.$$

2. We now use the Monte Carlo method to construct a critical region for T_n . Let B be the number of Monte Carlo iterations. For every $k = 1, \dots, B$,

- (a) if we know about the error distribution Z , then we draw $\boldsymbol{\epsilon}_{nk} \equiv (\epsilon_{1k}, \dots, \epsilon_{nk})'$ with all its components i.i.d. with distribution Z ;
- (b) if Z is not known, then we use the bootstrap method by drawing the bootstrap sample vector $\boldsymbol{\epsilon}_{nk}$ from $\{y_1 - \tilde{g}_n(\mathbf{X}_1), \dots, y_n - \tilde{g}_n(\mathbf{X}_n)\}$.

Then we compute only the local linear estimator based on the new observations $\{\mathbf{X}_j, \tilde{g}(\mathbf{X}_j) + \epsilon_{kj}\}_{j=1}^n$ using the same set of evaluation points (i.e. $\{\mathbf{x}_1, \dots, \mathbf{x}_m\}$) and the same bandwidth (i.e. \mathbf{h}_n) as before, which we denote by $\tilde{\tilde{g}}_{nk}$. Then, the modified bootstrap test statistic is

$$T_{nk} := \frac{1}{m} \sum_{i=1}^m \{\tilde{g}_n(\mathbf{x}_i) - \tilde{\tilde{g}}_{nk}(\mathbf{x}_i)\}^2.$$

3. The Monte Carlo p -value is defined as

$$p_n = \frac{1}{B} \sum_{k=1}^B \mathbf{1}\{T_n < T_{nk}\}.$$

For a test of size $\alpha \in (0, 1)$, we reject H_0 if $p_n < \alpha$.

A few remarks are in order. First, the intuition is that T_n should be small if $g_0 \in G_2$. Second, at first glance, we could define the bootstrap test statistic as

$$T_{nk}^* := \frac{1}{m} \sum_{i=1}^m \{\hat{g}_{nk}(\mathbf{x}_i) - \tilde{\tilde{g}}_{nk}(\mathbf{x}_i)\}^2,$$

where $\tilde{\tilde{g}}_{nk}$ and \hat{g}_{nk} are respectively the local linear estimator and SCKLS based on the

new observations $\{\mathbf{X}_j, \hat{g}(\mathbf{X}_j) + \epsilon_{jk}\}_{j=1}^n$. However, this would involve computing SCKLS B times, which is computationally expensive for large B . Instead, we note from the proof of Theorem 1 that

$$\frac{1}{m} \sum_{i=1}^m \{\hat{g}_n(\mathbf{x}_i) - \tilde{g}_n(\mathbf{x}_i)\}^2 \lesssim \frac{1}{m} \sum_{i=1}^m \{g_0(\mathbf{x}_i) - \tilde{g}_n(\mathbf{x}_i)\}^2$$

where \lesssim means smaller than or equal to in O_p . Therefore, we could use our modified bootstrap test statistics T_{nk} to approximate the distribution of the right hand side of the above equation, which only involves computing the local linear estimator B times, thus is computationally significantly faster.

The theoretical properties of our proposed test is presented below. Its proof can be found in Appendix C.

Theorem 6. *Suppose that Assumption 1(i),(ii),(iv)–(vi) and Assumption 2(ii) hold. Furthermore, assume that g_0 is twice-differentiable. Then, our test is consistent, i.e., under H_1 , for any $\alpha \in (0, 1)$, the probability of rejecting H_0 tends to 1 as $B \rightarrow \infty$ and $n \rightarrow \infty$.*

5.2 Testing for affinity

To further illustrate the usefulness of SCKLS for testing other shapes, we study the problem of testing

$$H_0 : g_0 : \mathbf{S} \rightarrow \mathbb{R} \text{ is affine} \quad \text{against} \quad H_1 : g_0 : \mathbf{S} \rightarrow \mathbb{R} \text{ is not affine.}$$

The main idea of our test is motivated by Sen and Meyer (2017). We show that under some regularity assumptions, our proposed test is consistent, i.e. under H_1 , its power goes to 1 as the sample size increases. Moreover, the critical value of the test can be easily computed using Monte Carlo or bootstrap methods. We now describe our testing procedure as follows.

1. First, we run linear regression on the response against the covariates and call the least squares fit g_n^L . Next, we fit the data using SCKLS (with evaluation points at $\mathbf{x}_1, \dots, \mathbf{x}_m$ and bandwidth \mathbf{h}_n). The resulting estimators are denoted by \hat{g}_n^V and \hat{g}_n^Λ , where \hat{g}_n^V is the SCKLS estimator using only a set of convexity constraints, while

\hat{g}_n^Λ is the SCKLS estimator using only a set of concavity constraints, all based on $\{\mathbf{X}_j, y_j\}_{j=1}^n$ ⁸. We then define the test statistics to be

$$T_n = \max \left[\frac{1}{m} \sum_{i=1}^m \{\hat{g}_n^V(\mathbf{x}_i) - g_n^L(\mathbf{x}_i)\}^2, \frac{1}{m} \sum_{i=1}^m \{\hat{g}_n^\Lambda(\mathbf{x}_i) - g_n^L(\mathbf{x}_i)\}^2 \right].$$

2. We simulate the distributional behavior of the test statistics B times under H_0 . For $k = 1, \dots, B$, we set the observations to be $\{\mathbf{X}_j, \epsilon_{jk}\}_{j=1}^n$ (so no change in the values of the covariates), where $\boldsymbol{\epsilon}_{nk} = (\epsilon_{1k}, \dots, \epsilon_{nk})'$ is drawn using the procedures as described in Section 5.1. Then we run linear regression on $\boldsymbol{\epsilon}_{nk}$ against the covariates and denote the least squares fit by g_{nk}^L . Fitting the data using SCKLS (with the same set of evaluation points and the same bandwidth as before) leads to the resulting estimators \hat{g}_{nk}^V and \hat{g}_{nk}^Λ , where \hat{g}_{nk}^V is the SCKLS estimator using only the convexity constraint, while \hat{g}_{nk}^Λ is the SCKLS estimator using only the concavity constraint, all based on $\{\mathbf{X}_j, \epsilon_{jk}\}_{j=1}^n$. So

$$T_{nk} = \max \left[\frac{1}{m} \sum_{i=1}^m \{\hat{g}_{nk}^V(\mathbf{x}_i) - g_{nk}^L(\mathbf{x}_i)\}^2, \frac{1}{m} \sum_{i=1}^m \{\hat{g}_{nk}^\Lambda(\mathbf{x}_i) - g_{nk}^L(\mathbf{x}_i)\}^2 \right].$$

3. The Monte Carlo p -value is defined as

$$p_n = \frac{1}{B} \sum_{k=1}^B \mathbf{1}_{\{T_n < T_{nk}\}}.$$

For a test of size $\alpha \in (0, 1)$, we reject H_0 if $p_n < \alpha$.

The intuition of the test is as follows. First, an affine function is both convex and concave, therefore under H_0 , both SCKLS estimates, \hat{g}_n^V and \hat{g}_n^Λ , should be close to the linear fit g_n^L , so the value of T_n should be small. In addition, a function is both convex and concave only if it is affine, so given enough observations, we should be able to reject the null hypothesis under H_1 . Finally, we used the fact that T_n based on $\{\mathbf{X}_j, y_j\}_{j=1}^n$ and $\{\mathbf{X}_j, \epsilon_j\}_{j=1}^n$ are exactly the same under H_0 to simulate the distributional behavior of T_n (see also Appendix C).

⁸For mathematical definitions of \hat{g}_n^V and \hat{g}_n^Λ see Appendix C.3

Theoretical property of our proposed test are presented below. Its proof can be found in Appendix C.

Theorem 7. *Suppose that Assumption 1(i),(ii),(iv)–(vi) and Assumption 2(ii) hold. Furthermore, assume that g_0 is twice-differentiable and the error distribution Z is known. Then for any $\alpha \in (0, 1)$, as $n \rightarrow \infty$ and $B \rightarrow \infty$,*

1. *if H_0 is true, then $P(p_n < \alpha) \rightarrow \alpha$;*
2. *if H_0 is false, then $P(p_n < \alpha) \rightarrow 1$.*

In other words, the test is approximately at most of size α and is consistent.

We remark that with proper choice of the bandwidth vector (e.g. see Assumption 1(vi)), our procedure alleviates the boundary issue of CNLS. Consequently, in our test procedure, there is no need to restrict further to the class of convex/concave functions with a fixed Lipschitz constant, a technical condition imposed by Sen and Meyer (2017).

Finally, in case we know that g_0 is monotonically increasing a priori, we could test H'_0 : g_0 is monotonically increasing and affine using essentially the same procedure with only minor modifications to gain power. More precisely, we instead run linear regression with signed constraints in both Step 1 and Step 2, replace \hat{g}_n^V by the SCKLS with both the convexity and monotonicity constraints, and \hat{g}_n^A by the SCKLS with both the concavity and monotonicity constraints.

6 Simulation study

6.1 Numerical experiments on estimation

6.1.1 The setup

In this section, we examine finite sample performance and robustness of the proposed estimator through Monte Carlo simulations. We run our experiments on a computer with Intel Core2 Quad CPU 3.00 GHz and 8GB RAM. The performance of SCKLS is compared with that of CWB and CNLS, as well as other model-specific competitors (whenever appropriate). For the SCKLS and the CNLS estimator, we solve the quadratic programming

problems with MATLAB using the built-in quadratic programming solver, `quadprog`. For the CWB estimator, we use the convex optimization solver `SeDuMi` because `quadprog` was not able to solve CWB⁹. We run six sets of experiments varying the size of noise, the distribution of the input variables, and investigate the effects of a non-uniform grid for imposing the shape constraints. Experiment 1 considers uniformly distributed input variables with a low noise level. Experiment 2 increases the noise level in the data generation process (DGP). Experiment 3 considers non-uniform distributed input variables to validate the robustness and the benefits of the extension of SCKLS: variable bandwidth with k -NN approach and non-uniform grid. Experiment 4 considers uniform input and vary the number of evaluation points to assess how the number of evaluation points affect the performance and computational difficulty of SCKLS and CWB estimator. Experiment 5 considers alternative concave/monotonic function which is generalized McFadden function to test the robustness of the SCKLS estimator for different shape of functions. In addition, we run the experiment where the true function is S-shape so the shape constrained estimators with concavity is misspecified, and report the results in Appendix E.5.

We measure the estimator’s performance using Root Mean Squared Errors (RMSE) based on two criteria: the distance from the estimated function to the true function measured 1) at the observed points and 2) at the evaluation points respectively. CNLS estimates hyperplanes at observation points and SCKLS estimates on evaluation points. We use linear interpolation to obtain the RMSE of CNLS¹⁰ and SCKLS on evaluation points and observation points respectively. We also measure how the iterative algorithm for SCKLS helps alleviate computational difficulty by reporting the percentage of constraints which are used to obtain the optimal solution and the computational time in seconds. We do not use the constraint reduction algorithm for CNLS. We replicate each scenario 10 times and report the average.

⁹For CWB, `SeDuMi` provides a better solution than `quadprog`, while both `SeDuMi` and `quadprog` give exactly the same solution for SCKLS.

¹⁰The CNLS estimates include the second stage linear programming estimation procedure described in Kuosmanen and Kortelainen (2012) to find the minimum extrapolated production function.

6.1.2 The choice of the tuning parameters

For both SCKLS and CWB estimators, we use the Gaussian kernel function $K(\cdot)$ and leave-one-out cross-validation (LOOCV) for bandwidth selection. LOOCV is a data-driven method, and has been shown to perform well for unconstrained kernel estimator such as local linear (Stone, 1977). Since SCKLS is numerically relatively insensitive to the bandwidth choice (see for example Section 6.1.3.1), to improve computational efficiency, here we apply LOOCV procedure on unconstrained estimates (i.e. Local Linear) to select the bandwidth for SCKLS with fixed bandwidth, SCKLS with variable bandwidth (i.e. on the choice of k for k -NN) and CWB. To further improve the computational performance, we apply the iterative algorithm described in Appendix D to both the SCKLS and CWB estimators. For CWB estimator, we use a local linear estimator to obtain the weighting matrix $A_j(\mathbf{x})$ in (2). The first partial derivative of $\hat{g}(\mathbf{x}|\mathbf{p})$ is obtained by approximating the derivatives through numerical differentiation $\hat{g}^{(1)}(\mathbf{x}|\mathbf{p}) = \frac{\hat{g}(\mathbf{x}+\Delta|\mathbf{p})-\hat{g}(\mathbf{x}|\mathbf{p})}{\Delta}$ where Δ is a small positive constant¹¹.

6.1.3 Results

6.1.3.1 Base Case: Uniform input – high signal-to-noise ratio

Experiment 1. We consider a Cobb–Douglas production function with d -inputs and one-output, $g_0(x_1, \dots, x_d) = \prod_{k=1}^d x_k^{\frac{0.8}{d}}$. For each pair (\mathbf{X}_j, y_j) , each component of the input, \mathbf{X}_{jk} , is randomly and independently drawn from uniform distribution $unif[1, 10]$, and the additive noise, ϵ_j , is randomly sampled from a normal distribution, $N(0, 0.7^2)$. We consider 15 different scenarios with different numbers of observations (100, 200, 300, 400 and 500) and input dimension (2, 3 and 4). The structure and data generation process of Experiment 1 follows Lee et al. (2013). The number of evaluation points is fixed at 400, and set as a uniform grid.

For this experiment, we compare the following five estimators: SCKLS with the fixed (i.e. location-independent) LOOCV bandwidth, CNLS, CWB in p -space, Local Linear

¹¹Du et al. (2013) proposes to use an analytical derivative for the first partial derivative of $\hat{g}(\mathbf{x}|\mathbf{p})$; however, the analytical derivative performs similarly to numerical differentiation as shown in Racine (2016). We propose two alternative methods to compute the first partial derivative, and compared them in Appendix A.1.

Kernel, and parametric Cobb–Douglas function. Table 1 and 2 show for Experiment 1 the RMSE measured on observation points and evaluation points respectively. The number in parentheses is the standard deviation of RMSE calculated from 10 replications. Note the standard deviation are generally small compared to the parameter estimates indicating even after only 10 replications the variability in the estimates is low. A more extensive set of results for this experiment is summarized in Appendix E.1. The SCKLS estimator has the lowest root RMSE in most scenarios even when RMSE is measured on observation points (note the SCKLS estimator imposes the shape constraints on evaluation points in Equation (6)). Also as expected, the performance of SCKLS estimator improves as the number of observation points increases. Moreover, the SCKLS estimator performs better than the Local Linear estimator particularly in higher dimensional functional estimation. Thus, providing empirically evidence that the shape constraints in the SCKLS estimator are helpful to improve the finite sample performance. Note that the Local Linear estimator has larger RMSE values on evaluation points which are located in input space regions with sparse observations. This implies that the SCKLS estimator has more robust out-of-sample performance than the Local Linear estimator due to the shape constraints. We also observe that the performance of the CNLS estimator measured at the evaluation points is worse than that measured at the observations. CNLS often has ill-defined hyperplanes which are very steep/shallow at the edge of the observed data, this over fitting leads to poor out-of-sample performance. In contrast, the SCKLS estimator performs similarly for both the observation points and evaluation points due to the construction of the grid that completely covers the observed data making the SCKLS estimator more robust. Although the SCKLS and the CWB estimators are relatively competitive when the number of observations is large, the SCKLS estimator has significantly better performance when the observations are smaller and in higher dimension.

Table 3 shows the computational time of Experiment 1 for the shape constrained estimators which are more computationally intensive than the Local Linear estimator. The value inside parenthesis indicates the percentage of constraints included in the optimization problem that resulted in the optimal solution. While CNLS is the fastest estimator when the number of observations is small, the SCKLS estimator could be faster in the case of

larger datasets or high dimensional scenarios. Since we alleviate the curse of dimensionality by using the iterative algorithm, we can analyze larger dataset to estimate production function. The iterative algorithm is more effective for estimating low dimensionality functions because in higher dimensional spaces the number of adjacent grid points is relatively large.

We also conduct simulations with different bandwidths to analyze the sensitivity of each estimator to bandwidths. We estimate SCKLS with fixed bandwidth, CWB in p -space and Local Linear with bandwidth $h \in [0, 10]$ with an increment by 0.01 for 1-input setting, and we use bandwidth $\mathbf{h} \in [0, 5] \times [0, 5]$ with an increment by 0.25 for 2-input setting. We perform 100 simulations for each bandwidth, and compute the optimal bandwidth with LOOCV for each simulation. Figure 3 displays the average RMSE of each estimator. The distribution of bandwidths selected by LOOCV are shown in the histogram. The instances when SCKLS, CWB- p , and Local Linear provide the lowest RMSE are shown in light gray, gray and dark gray respectively on the histogram. For one-input scenario, the SCKLS and CWB estimator perform similar for bandwidth between 0.25 - 2.25 as shown by the

Table 1. RMSE on observation points for Experiment 1.

Number of observations	Average of RMSE on observation points					
	100	200	300	400	500	
2-input	SCKLS	0.193 (0.053)	0.171 (0.047)	0.141 (0.032)	0.132 (0.029)	0.118 (0.017)
	CNLS	0.229 (0.042)	0.163 (0.037)	0.137 (0.010)	0.138 (0.027)	0.116 (0.016)
	CWB in p -space	0.189 (0.055)	0.167 (0.049)	0.158 (0.040)	0.140 (0.026)	0.129 (0.019)
	Local Linear	0.212 (0.079)	0.166 (0.042)	0.149 (0.028)	0.152 (0.028)	0.140 (0.028)
	Cobb–Douglas	0.078	0.075	0.048	0.039	0.043
3-input	SCKLS	0.230 (0.050)	0.187 (0.026)	0.183 (0.032)	0.152 (0.019)	0.165 (0.031)
	CNLS	0.294 (0.048)	0.202 (0.035)	0.189 (0.020)	0.173 (0.014)	0.168 (0.020)
	CWB in p -space	0.228 (0.043)	0.221 (0.039)	0.210 (0.037)	0.183 (0.040)	0.172 (0.024)
	Local Linear	0.250 (0.068)	0.230 (0.050)	0.235 (0.052)	0.203 (0.050)	0.181 (0.021)
	Cobb–Douglas	0.104	0.089	0.070	0.047	0.041
4-input	SCKLS	0.225 (0.038)	0.248 (0.020)	0.228 (0.037)	0.203 (0.042)	0.198 (0.028)
	CNLS	0.315 (0.039)	0.294 (0.027)	0.246 (0.024)	0.235 (0.029)	0.214 (0.015)
	CWB in p -space	0.238 (0.038)	0.262 (0.056)	0.231 (0.039)	0.234 (0.076)	0.198 (0.030)
	Local Linear	0.256 (0.044)	0.297 (0.057)	0.252 (0.056)	0.240 (0.060)	0.226 (0.038)
	Cobb–Douglas	0.120	0.073	0.091	0.067	0.063

Table 2. RMSE on evaluation points for Experiment 1.

Number of observations		Average of RMSE on evaluation points				
		100	200	300	400	500
2-input	SCKLS	0.219 (0.053)	0.189 (0.057)	0.150 (0.034)	0.147 (0.030)	0.128 (0.021)
	CNLS	0.350 (0.082)	0.299 (0.093)	0.260 (0.109)	0.284 (0.119)	0.265 (0.078)
	CWB in p -space	0.206 (0.049)	0.186 (0.062)	0.174 (0.043)	0.154 (0.026)	0.143 (0.021)
	Local Linear	0.247 (0.101)	0.182 (0.053)	0.167 (0.030)	0.171 (0.030)	0.156 (0.034)
	Cobb–Douglas	0.076	0.076	0.049	0.040	0.043
3-input	SCKLS	0.283 (0.072)	0.231 (0.033)	0.238 (0.030)	0.213 (0.029)	0.215 (0.034)
	CNLS	0.529 (0.112)	0.587 (0.243)	0.540 (0.161)	0.589 (0.109)	0.598 (0.143)
	CWB in p -space	0.291 (0.069)	0.289 (0.052)	0.269 (0.035)	0.252 (0.052)	0.233 (0.031)
	Local Linear	0.336 (0.085)	0.340 (0.093)	0.360 (0.108)	0.326 (0.086)	0.264 (0.042)
	Cobb–Douglas	0.116	0.098	0.080	0.052	0.046
4-input	SCKLS	0.321 (0.046)	0.357 (0.065)	0.329 (0.049)	0.308 (0.084)	0.290 (0.044)
	CNLS	0.845 (0.188)	0.873 (0.137)	0.901 (0.151)	0.827 (0.235)	0.792 (0.091)
	CWB in p -space	0.360 (0.039)	0.385 (0.077)	0.358 (0.068)	0.361 (0.138)	0.325 (0.077)
	Local Linear	0.482 (0.115)	0.527 (0.125)	0.483 (0.146)	0.495 (0.153)	0.445 (0.074)
	Cobb–Douglas	0.146	0.091	0.115	0.081	0.080

Table 3. Computational time for Experiment 1.

		The average computational time in seconds; (percentage of Afriat constraints included in the final optimization)				
Number of observations		100	200	300	400	500
2-input	SCKLS	14.1 (6.14%)	13.3 (5.28%)	42.2 (8.86%)	34.7 (7.80%)	77.4 (8.31%)
	CNLS	2.0 (100.00%)	6.1 (100.00%)	16.5 (100.00%)	26.5 (100.00%)	55.3 (100.00%)
	CWB in p -space	24.1 (2.39%)	33.2 (2.35%)	76.6 (2.35%)	82.3 (2.35%)	130 (2.35%)
3-input	SCKLS	26.9 (16.00%)	40.4 (16.60%)	45.5 (16.30%)	67.3 (16.40%)	136 (16.20%)
	CNLS	3.8 (100.00%)	16.4 (100.00%)	37 (100.00%)	82.9 (100.00%)	161 (100.00%)
	CWB in p -space	47.6 (15.50%)	71.5 (15.50%)	100 (15.50%)	202 (15.50%)	255 (15.50%)
4-input	SCKLS	47.5 (40.10%)	71.6 (39.90%)	77.4 (39.90%)	166 (40.00%)	235 (39.80%)
	CNLS	5.8 (100.00%)	22.4 (100.00%)	79.1 (100.00%)	139.8 (100.00%)	287.8 (100.00%)
	CWB in p -space	68.8 (39.80%)	136 (39.80%)	196 (39.80%)	327 (39.80%)	442 (39.80%)

closeness of the light gray and gray curves in (a). In contrast, for two-input scenario, the SCKLS estimator performs better for most of the LOOCV values as shown by the majority of the histogram colored in light gray. This indicates that LOOCV calculate for unconstrained estimator provide bandwidths that work well for the SCKLS estimator. Moreover, the SCKLS estimator is not very sensitive to the bandwidth selection method since heuristically the shape constraints help reduce the variance of the estimator.

6.1.3.2 Uniform input – low signal-to-noise ratio

Experiment 2. We consider a Cobb–Douglas production function with d -inputs and one-output, $g_0(x_1, \dots, x_d) = \prod_{k=1}^d x_k^{\frac{0.8}{d}}$. For each pair (\mathbf{X}_j, y_j) , each component of the input, \mathbf{X}_{jk} , is randomly and independently drawn from uniform distribution $unif[1, 10]$, and the additive noise, ϵ_j , is randomly and independently sampled from a normal distribution, $N(0, 1.3^2)$. We consider 15 different scenarios with different numbers of observations (100, 200, 300, 400 and 500) and input dimension (2, 3 and 4). The number of evaluation points is fixed at 400, and set as a uniform grid. This experiment has a higher noise level in the data generation process relative to Experiment 1.

For this experiment, we compare the same five estimators: SCKLS with the fixed

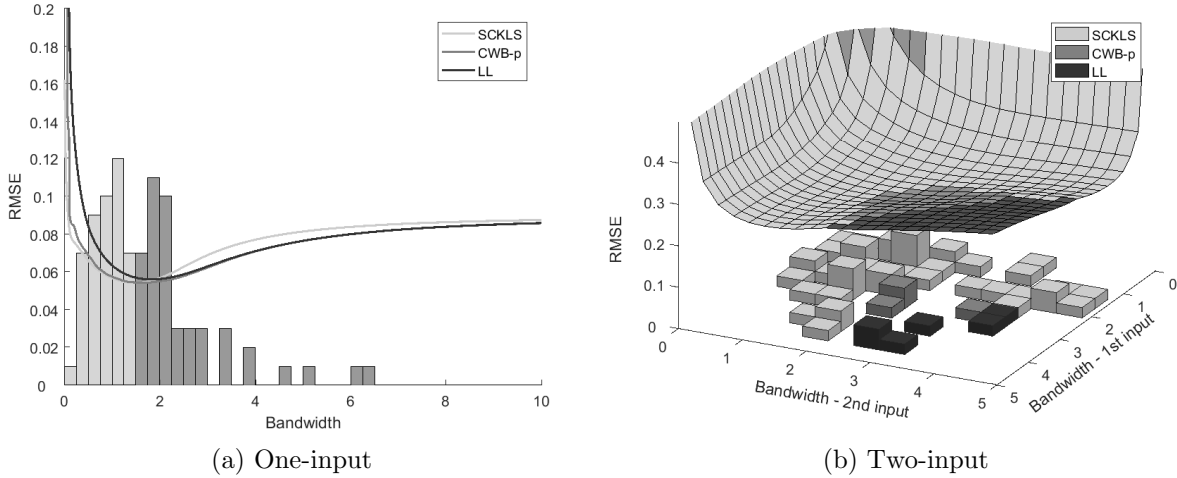


Figure 3. The histogram shows the distribution of bandwidths selected by LOOCV. The curves show the relative performance of the three estimators.

Table 4. RMSE on observation points for Experiment 2.

Number of observations		Average of RMSE on observation points				
		100	200	300	400	500
2-input	SCKLS	0.239	0.203	0.203	0.155	0.140
	CNLS	0.279	0.231	0.194	0.168	0.151
	CWB in p -space	0.314	0.215	0.237	0.275	0.151
	Local Linear	0.287	0.244	0.230	0.214	0.161
	Cobb–Douglas	0.109	0.108	0.081	0.042	0.048
3-input	SCKLS	0.292	0.263	0.221	0.204	0.184
	CNLS	0.379	0.303	0.275	0.224	0.214
	CWB in p -space	0.318	0.306	0.308	0.244	0.214
	Local Linear	0.333	0.306	0.288	0.259	0.214
	Cobb–Douglas	0.176	0.118	0.101	0.084	0.072
4-input	SCKLS	0.317	0.291	0.249	0.241	0.254
	CNLS	0.491	0.356	0.311	0.293	0.313
	CWB in p -space	0.400	0.318	0.273	0.260	0.289
	Local Linear	0.335	0.342	0.257	0.274	0.283
	Cobb–Douglas	0.157	0.150	0.112	0.075	0.077

LOOCV bandwidth, CNLS, CWB in p -space, Local Linear Kernel, and parametric Cobb–Douglas function. Table 4 and 5 summarizes the estimators’ performance for Experiment 2 in terms of RMSE measured on observation points and evaluation points respectively. The comprehensive results of this experiment is summarized in Appendix E.2. In contrast to Experiment 1, CWB is not stable or competitive relative to the SCKLS estimator. The CWB estimator first estimates the unconstrained kernel weighted estimator, and this first stage estimate can deviate from the true function significantly in the high noise scenarios. Because the second stage of the CWB estimator identifies the shape restricted function as

Table 5. RMSE on evaluation points for Experiment 2.

Number of observations		Average of RMSE on evaluation points				
		100	200	300	400	500
2-input	SCKLS	0.253	0.225	0.222	0.172	0.160
	CNLS	0.319	0.355	0.334	0.255	0.267
	CWB in p -space	0.329	0.239	0.262	0.305	0.177
	Local Linear	0.330	0.272	0.257	0.239	0.194
	Cobb–Douglas	0.112	0.112	0.083	0.044	0.049
3-input	SCKLS	0.367	0.339	0.302	0.268	0.231
	CNLS	0.743	0.778	0.744	0.696	0.620
	CWB in p -space	0.398	0.392	0.434	0.336	0.274
	Local Linear	0.452	0.444	0.438	0.398	0.302
	Cobb–Douglas	0.202	0.130	0.110	0.093	0.079
4-input	SCKLS	0.405	0.460	0.349	0.350	0.347
	CNLS	1.019	0.950	0.985	1.043	1.106
	CWB in p -space	0.514	0.520	0.393	0.390	0.452
	Local Linear	0.524	0.626	0.451	0.491	0.550
	Cobb–Douglas	0.187	0.194	0.134	0.092	0.091

close as possible to the unrestricted estimator, a poor estimate in the first stage leads to poor performance of the CWB estimator overall. This indicates that the SCKLS estimator is more robust to the noise in data than CWB estimator.

6.1.3.3 Non-uniform input

Experiment 3. We consider a Cobb–Douglas production function with d -inputs and one-output, $g_0(x_1, \dots, x_d) = \prod_{k=1}^d x_k^{\frac{0.8}{d}}$. For each pair (\mathbf{X}_j, y_j) , each component of the input, \mathbf{X}_{jk} , is randomly and independently drawn from a truncated exponential distribution with density function $f(x) = \frac{3}{e^{-3} - e^{-30}} e^{-3x} I_{\{x \in [1, 10]\}}$, and the additive noise, ϵ_j , is randomly sampled from a normal distribution, $N(0, 0.7^2)$. We consider 15 different scenarios with different numbers of observations (100, 200, 300, 400 and 500) and input dimension (2, 3 and 4). The number of evaluation point is fixed at 400. Note this experiment only differs from Experiment 1 in that the distribution of inputs is skewed and thus non-uniform.

For this experiment, we compare the performance of SCKLS estimator with different extensions: SCKLS with fixed LOOCV bandwidth, with variable bandwidth (k -NN) and with non-uniform grid. Table 6 and 7 show the RMSE of Experiment 3 on observation points and evaluation points respectively. The comprehensive results of this experiment is summarized in Appendix E.3. A uniform grid is used like in Experiment 1. As the dimension of input space and the number of observations increase, SCKLS with variable

Table 6. RMSE on observation points for Experiment 3.

Number of observations		Average of RMSE on observation points				
		100	200	300	400	500
2-input	SCKLS fixed/uniform	0.179	0.151	0.144	0.121	0.108
	SCKLS variable/uniform	0.183	0.156	0.142	0.125	0.104
	SCKLS variable/non-uniform	0.176	0.144	0.132	0.114	0.093
3-input	SCKLS fixed/uniform	0.197	0.184	0.172	0.164	0.167
	SCKLS variable/uniform	0.212	0.187	0.170	0.175	0.170
	SCKLS variable/non-uniform	0.210	0.180	0.162	0.160	0.155
4-input	SCKLS fixed/uniform	0.219	0.211	0.196	0.209	0.187
	SCKLS variable/uniform	0.208	0.193	0.167	0.171	0.170
	SCKLS variable/non-uniform	0.206	0.193	0.164	0.169	0.168

Table 7. RMSE on evaluation points for Experiment 3.

Number of observations		Average of RMSE on evaluation points				
		100	200	300	400	500
2-input	SCKLS fixed/uniform	0.262	0.220	0.244	0.157	0.196
	SCKLS variable/uniform	0.246	0.204	0.192	0.142	0.136
	SCKLS variable/non-uniform	0.193	0.160	0.145	0.120	0.100
3-input	SCKLS fixed/uniform	0.323	0.308	0.311	0.286	0.293
	SCKLS variable/uniform	0.335	0.303	0.281	0.262	0.254
	SCKLS variable/non-uniform	0.278	0.243	0.219	0.212	0.196
4-input	SCKLS fixed/uniform	0.406	0.398	0.397	0.404	0.400
	SCKLS variable/uniform	0.417	0.423	0.368	0.364	0.356
	SCKLS variable/non-uniform	0.359	0.359	0.313	0.302	0.280

bandwidth performs better than the fixed bandwidth estimator. SCKLS with non-uniform grid performs better than SCKLS with uniform grid for almost all scenarios, largely due to the fact that the DGP has non-uniform input. Consequently, we conclude that variable bandwidth methods, such as k -NN approach, and non-uniform grid could be useful to handle skewed input data which is a common feature of census manufacturing data which is the type of data we consider in the application, Section 7.

6.1.3.4 Different numbers of evaluation points

Experiment 4. The setting is exactly same as Experiment 1. However, now we consider 9 different scenarios with different numbers of evaluation points (100, 300 and 500) and input dimension (2, 3 and 4). The number of observations is fixed at 400. The evaluation points are constructed on a uniform grid.

We compare following two estimators: SCKLS with fixed bandwidth, CWB in p -space. Table 8 and 9 shows for Experiment 4 the RMSE measured on observations and evaluation points respectively. The comprehensive results of this experiment is summarized in

Appendix E.3. The SCKLS estimator outperforms the CWB estimator for almost all scenarios. Table 8 shows that even if we increase the number of evaluation points, the RMSE value does not change significantly. This has important implications for the running time. Specifically, we can reduce the calculation time by using a rough grid without sacrificing too much in terms of RMSE performance of the estimator.

Table 10 summarizes the computational times for Experiment 4 and shows the percentage of constraints used for each estimator. The SCKLS estimator can always be calculated faster than the CWB estimator. When the dimensionality of the input space is low, the number of evaluation points does not affect the computational time much because the iterative algorithm reduce the number of constraints significantly. However, when the dimensionality is high, the large number of adjacent grid points creates a large number of constraints and thus a single quadratic program takes a long time to solve. Summarizing the results from Experiment 4, we recommend using a rough grid in high dimensional input data cases to keep computational times reasonably short.

6.1.3.5 Alternative concave/monotonic Function

Experiment 5. We perform experiments with an alternative functional form that satisfy the global monotonicity and concavity. We use the Generalized McFadden function as the

Table 8. RMSE on observation points for Experiment 4.

Number of evaluation points		Average of RMSE on observation points		
		100	300	500
2-input	SCKLS	0.142	0.141	0.141
	CWB in p -space	0.149	0.151	0.156
3-input	SCKLS	0.198	0.203	0.197
	CWB in p -space	0.218	0.234	0.231
4-input	SCKLS	0.239	0.207	0.206
	CWB in p -space	0.219	0.227	0.296

Table 9. RMSE on evaluation points for Experiment 4.

Number of evaluation points		Average of RMSE on evaluation points		
		100	300	500
2-input	SCKLS	0.181	0.164	0.158
	CWB in p -space	0.195	0.180	0.179
3-input	SCKLS	0.304	0.267	0.257
	CWB in p -space	0.332	0.329	0.302
4-input	SCKLS	0.383	0.296	0.270
	CWB in p -space	0.403	0.359	0.415

Table 10. Computational time for Experiment 4.

Number of evaluation points		The average computational time in seconds; (percentage of Afriat constraints included in the final optimization)		
		100	300	500
2-input	SCKLS	26.6 (11.7%)	28.3 (6.6%)	34.0 (5.4%)
	CWB in p -space	41.0 (8.8%)	56.5 (3.2%)	74.2 (2.0%)
3-input	SCKLS	84.8 (29.1%)	111.7 (16.7%)	134.1 (13.3%)
	CWB in p -space	120.5 (28.2%)	221.0 (15.5%)	309.9 (12.2%)
4-input	SCKLS	149.1 (62.3%)	169.5 (40.0%)	597.3 (27.7%)
	CWB in p -space	174.6 (61.9%)	274.6 (39.8%)	729.2 (27.4%)

DGP. For $\mathbf{x} = (x_1, \dots, x_d)'$,

$$g_0(\mathbf{x}) = \frac{1}{2} \cdot \frac{\mathbf{x}'\mathbf{C}\mathbf{x}}{\boldsymbol{\theta}'\mathbf{x}} + \sum_{k=1}^d \beta_k x_k \quad (11)$$

where $\mathbf{C} = -\mathbf{A}\mathbf{A}'$ and \mathbf{A} is $d \times d$ lower triangular matrix, and thus, \mathbf{C} is negative semidefinite. We set all the diagonal elements of \mathbf{A} to be 1.0, and all the lower triangular elements of \mathbf{A} to be 0.4. $\boldsymbol{\theta}$ is $d \times 1$ -vector whose value is the mean of input vector \mathbf{X}_j . For the details of generalized McFadden function, see Diewert and Wales (1987) and Nemoto and Goto (2004). Here for $j = 1, \dots, n$, each component of the input, \mathbf{X}_{jk} (for $k = 1, \dots, d$), is randomly and independently drawn from uniform distribution $unif[1, 10]$, and random noise, ϵ_j , is randomly and independently sampled from a normal distribution, $N(0, 0.7^2)$.

Table 11 and 12 show the RMSE of this experiment on observation points and evaluation points, respectively. In most scenarios, the SCKLS estimator either has the best performance or is at least competitive with other estimators. In general, our experience suggests that SCKLS is robust to different functional forms which are globally concave and monotonic.

Table 11. RMSE on observation points for Experiment 5

Number of observations		Average of RMSE on observation points				
		100	200	300	400	500
2-input	SCKLS fixed bandwidth	0.180	0.141	0.138	0.144	0.135
	CNLS	0.227	0.166	0.139	0.147	0.126
	CWB in p -space	0.213	0.179	0.158	0.205	0.241
3-input	SCKLS fixed bandwidth	0.259	0.208	0.194	0.174	0.171
	CNLS	0.288	0.226	0.197	0.173	0.174
	CWB in p -space	0.345	0.346	0.278	0.252	0.284
4-input	SCKLS fixed bandwidth	0.306	0.288	0.302	0.286	0.285
	CNLS	0.347	0.310	0.285	0.287	0.284
	CWB in p -space	0.383	0.358	0.371	0.502	0.371

Table 12. RMSE on evaluation points for Experiment 5

Number of observations		Average of RMSE on evaluation points				
		100	200	300	400	500
2-input	SCKLS fixed bandwidth	0.200	0.154	0.157	0.163	0.159
	CNLS	0.685	0.724	0.824	0.901	0.681
	CWB in p -space	0.241	0.198	0.184	0.245	0.275
3-input	SCKLS fixed bandwidth	0.314	0.248	0.262	0.211	0.213
	CNLS	1.507	1.158	1.492	1.344	1.275
	CWB in p -space	0.413	0.422	0.367	0.356	0.370
4-input	SCKLS fixed bandwidth	0.443	0.417	0.421	0.393	0.386
	CNLS	2.246	1.484	1.073	1.152	0.883
	CWB in p -space	0.563	0.516	0.565	0.669	0.548

6.2 Numerical experiments on testing

6.2.1 Testing for monotonicity and concavity

Experiment 6. We test monotonicity and concavity for data generated from the following DGP:

$$g_0(\mathbf{x}) = \frac{1}{d} \sum_{k=1}^d x_k^p \quad (12)$$

and

$$g_0(\mathbf{x}) = \frac{1}{d} \sum_{k=1}^d \frac{1}{1 + \exp(-5 \log(2x_k))} \quad (13)$$

where $\mathbf{x} = (x_1, \dots, x_d)'$. With n observations, for each pair (\mathbf{X}_j, y_j) , each component of the input, \mathbf{X}_{jk} , is randomly and independently drawn from uniform distribution $unif[0, 1]$, and the additive noise, ϵ_j , is randomly and independently sampled from a normal distribution, $N(0, 0.1)$. For the DGP with function (12), the exponent parameter p defines whether function is concave, convex or linear. We use $p = \{0.2, 0.5, 1.0, 2.0, 5.0\}$ where the function is concave if $p < 1$, convex if $p > 1$ and affine if $p = 1$. On the other hand, the function

defined by (13) is an “S”-shape function which violates both global concavity and convexity. We consider different sample sizes $n = \{100, 300, 500\}$ and vary the number of inputs $d = \{1, 2\}$, and perform 100 simulations to compute the rejection rate for each scenario. We assume that we do not know the distribution of the noise in advance and use the bootstrap procedure described in Section 5.1 with $B = 500$. The comprehensive results of this experiment is summarized in Appendix E.6.

Table 13 shows the rejection rate for each DGP with one-input ($d = 1$) and two-input ($d = 2$) scenarios. For one-input scenarios, the test works well even when the sample size is small. Both type I and type II errors of our test is small. Thus, this test appears robust enough to guide users to avoid imposing shape constraints on the data generated from misspecified functions. Furthermore, for two-input scenarios in our settings, the rejection rate under H_1 significantly improves when the sample size is increased from 100 to 300. Indeed, as we move to higher dimensions, more data is required for the test to gain enough power.

Table 13. Rejection rate of the test for monotonicity and concavity

Sample size (n)	Shape Parameter (p)	Power of the Test (α)			
		$d = 1$		$d = 2$	
		0.05	0.01	0.05	0.01
100	0.2	0.00	0.00	0.00	0.00
	0.5	0.00	0.00	0.01	0.00
	1.0	0.00	0.00	0.05	0.01
	2.0	1.00	1.00	0.93	0.82
	5.0	1.00	1.00	1.00	1.00
	S-shape	1.00	0.97	0.64	0.42
300	0.2	0.00	0.00	0.00	0.00
	0.5	0.00	0.00	0.00	0.00
	1.0	0.00	0.00	0.03	0.00
	2.0	1.00	1.00	1.00	1.00
	5.0	1.00	1.00	1.00	1.00
	S-shape	1.00	1.00	0.99	0.98
500	0.2	0.00	0.00	0.00	0.00
	0.5	0.00	0.00	0.00	0.00
	1.0	0.00	0.00	0.01	0.00
	2.0	1.00	1.00	1.00	1.00
	5.0	1.00	1.00	1.00	1.00
	S-shape	1.00	1.00	1.00	1.00

6.2.2 Testing for affinity

Experiment 7. We consider the affinity test with data generated from the function defined in (12). We consider different sample sizes $n = \{100, 300, 500\}$ and vary the number of inputs $d = \{1, 2\}$, and perform 100 simulations to compute the rejection rate for each scenario. We assume that we do not know the distribution of the noise in advance and use the bootstrap method outlined in Section 5.2 with $B = 500$.

Table 14 show the rejection rate for each scenario with one-input and two-input. Again we note that the proposed test works well with a moderate sample size.

Table 14. Rejection rate of the test for affinity

Sample size (n)	Shape Parameter (p)	Power of the Test (α)			
		$d = 1$		$d = 2$	
		0.05	0.01	0.05	0.01
100	0.2	0.99	0.95	0.74	0.57
	0.5	0.97	0.92	0.79	0.57
	1.0	0.05	0.00	0.02	0.00
	2.0	1.00	1.00	1.00	0.99
	5.0	1.00	1.00	1.00	1.00
300	0.2	1.00	1.00	1.00	1.00
	0.5	1.00	1.00	0.99	0.99
	1.0	0.05	0.00	0.01	0.00
	2.0	1.00	1.00	1.00	1.00
	5.0	1.00	1.00	1.00	1.00
500	0.2	1.00	1.00	1.00	1.00
	0.5	1.00	1.00	1.00	1.00
	1.0	0.08	0.02	0.01	0.00
	2.0	1.00	1.00	1.00	1.00
	5.0	1.00	1.00	1.00	1.00

7 Application

We apply the proposed method to estimate the production function for two large industries in Chile: plastic (2520) and wood manufacturing (2010) where the values inside the parentheses indicate CIU3 industry code. There are some existing studies which analyze the productivity of Chilean data, see for example Pavcnik (2002). She analyzed how trade liberalization affects the productivity improvements. Other researchers have analyzed the productivity of Chilean manufacturing including Benavente (2006), Benavente and Ferrada (2003), Alvarez and Robertson (2004), Alvarez and Görg (2009) and De Loecker (2007).

However, the above-cited work use strong parametric assumptions and older data. Here, we relax the parametric assumptions and estimate a shape constrained production function nonparametrically using data from 2010. We examine the marginal productivity, marginal rate of substitution and most productive scale size (MPSS) to analyze the structure using nonparametric estimation. Furthermore, we also investigate how productivity differs between exporting and non-exporting firms¹², as exporting has become an important source of revenue in Chile.

7.1 The census of Chilean manufacturing plants

We use the Chilean Annual Industrial Survey which is provided by National Institute of Statistics in Chile¹³. The survey of the census covers manufacturing establishments with ten or more employees. We define Capital and Labor as the input variables and Value Added as the output variable of the production function. Capital and Value Added are measured in millions of Chilean peso while Labor is measured as the total man-hours per year. We use cross sectional data from two large industries in Chilean manufacturing industry, namely, plastic and wood.

Many researchers have found positive effects of exporting for other countries using parametric models. See for instance, De Loecker (2007) and Bernard and Jensen (2004). Here we use SCKLS to relax the parametric assumption for the production function. To capture the effects of exporting, we use a semi-parametric modeling extension of SCKLS described in Appendix F, see also Robinson (1988). We model exporting with two variables: a dummy variable indicating the establishments that are exporting and the share of output being exported. Our empirical results indicate exporting establishments are more productive than non-exporters establishments.

Table 15 presents the summary of statistics for each industry by exporter/non-exporter.

¹²Note firms decisions are potentially endogenous. This means to the extent that the firms considers demand shocks and other components of the residual when selecting labor and capital levels or whether to export, our estimates may suffer from the endogeneity problem describe by Marschak and Andrews (1944). Solutions to this issue are to instrument or build a structural model based on timing assumptions. See Akerberg et al. (2015) for a recent discussion of the issue. Therefore, our results are better suited for prediction rather than a casual interpretation.

¹³Data is available at National Institute of Statistics in Chile (http://www.ine.cl/canales/chile_estadistico/estadisticas_economicas/industria/series_estadisticas/series_estadisticas_enia.php).

Table 15. Statistics of Chilean manufacturing data.

Plastic (2520)	Non-exporters ($n = 173$)			Exporters ($n = 72$)			
	Labor	Capital	Value	Labor	Capital	Value	Share of Exports
		(million)	Added (million)		(million)	(million)	
mean	92155	725.85	546.93	240890	2859	1733.9	0.147
median	55220	258.41	247.05	180330	1329.1	1054.9	0.0524
std	106530	1574	1068.1	212480	3840.2	1678.8	0.201
skewness	3.301	5.2052	5.9214	1.3681	2.4594	1.0678	-0.303
Wood (2010)	Non-exporters ($n = 97$)			Exporters ($n = 35$)			
	Labor	Capital	Value	Labor	Capital	Value	Share of Exports
		(million)	Added (million)		(million)	(million)	
mean	76561	364.93	334.83	501470	3063.4	4524.1	0.542
median	44087	109.48	115.39	378000	2195.4	2673.5	0.648
std	78057	702.35	555.87	436100	2510.3	4466.3	0.355
skewness	2.243	3.5155	3.432	0.81454	0.63943	1.0556	-0.303

We find that exporters are typically larger than non-exporter in terms of labor and capital. Input variables are positively skewed, indicating there exist many small and few large establishments. Since SCKLS with variable bandwidth (k -NN) and non-uniform grid performed the best in our simulation scenarios with non-uniform input data, we use these options in the analysis here.

Figure 4 is a plot of labor and capital for each industry, where we find that input data is sparse for large establishments. Beresteanu (2005) proposed to include shape constraints only for the evaluation points that contain at least one observation within a gridded square. So in addition to using a non-uniform grid of evaluation points, we also apply Beresteanu criteria to avoid using redundant evaluation points and over smoothing.

7.2 Estimated production function and interpretation

We estimate a semi-parametric model with a nonparametric shape constrained production function and a linear model for exporting share of sales and a dummy variables of exporting. Table 16 shows the goodness of fit of the production function: 71.1% of variance is explained in plastic industry while 43.8% of variance is explained in wood industry.

Table 16. SCKLS fitting statistics for Cross Sectional data.

Industry	Number of observations	Fraction of variance explained
Plastic	245	71.1%
Wood	132	43.8%

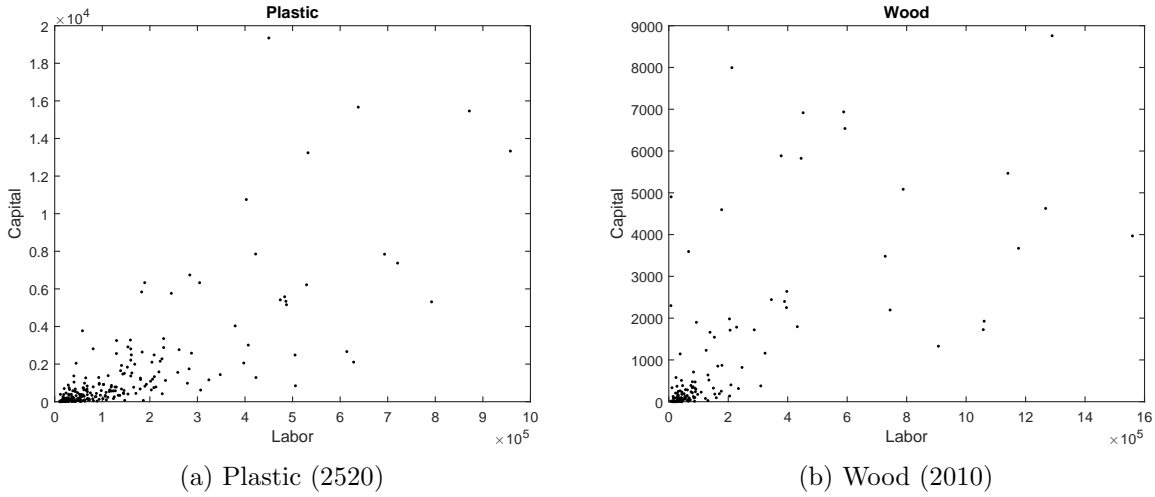


Figure 4. Labor and Capital of each industry.

Table 17 reports additional information characterizing the production function: the marginal productivity and the marginal rates of substitution at the 10, 25, 50, 75 and 90 percentiles are reported for both measures. Here, the rate of substitution indicates that how much labor is required to maintain the same level of output when we decrease a unit of capital. Figure 5 includes graphs of the estimated production functions. Comparing the two industries, the wood industry has a larger marginal rate of substitution than the plastic industry. This indicates that capital is more critical in wood industry than plastic industry. This result is also apparent in Figure 5, where it appears that the production function of wood industry is not particularly sensitive to changes in labor.

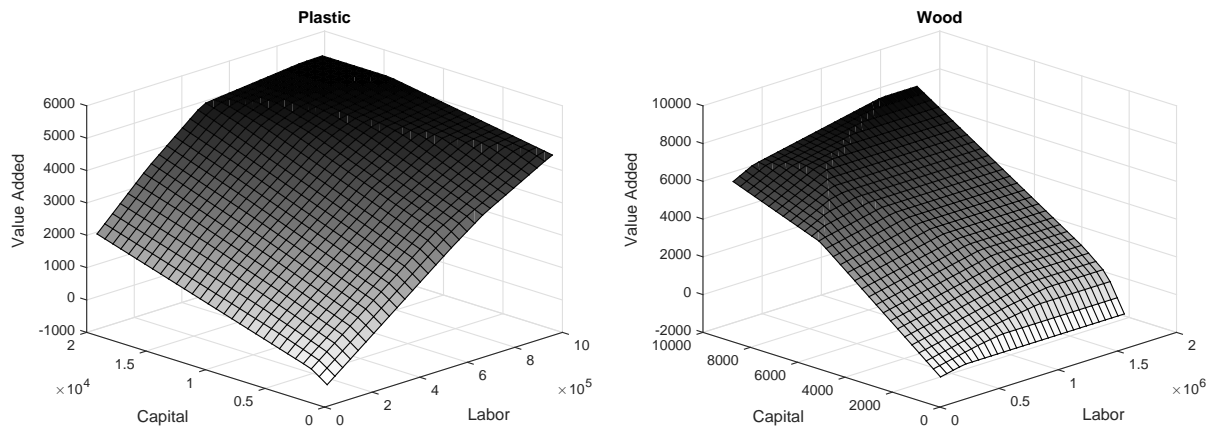
Table 18 reports the estimated coefficients for the exporting variables. In the plastic industry, the dummy variable for exporting is significant and positive while exports' share of sales is not. This indicates that the plants that export tend to produce more output than plants who do not export regardless of the export quantity. In contrast, the coefficient on the exports' share of sales is significant and positive in wood industry while dummy variable for exporting is not significant indicating the establishments in wood industry tend to be more productive the more they export. Thus in both industries we find evidence of increased productivity for exporting firms.

Table 19 reports the most productive scale size for the 10, 25, 50 75, 90 percentiles of Capital/Labor ratio distribution of observed input. In both industries, the observed value

Table 17. Characteristics of production function.

Plastic (2520)			
	Marginal Productivity		Marginal Rate of Substitution
	Labor ($= b_l$) (million peso/man hours)	Capital ($= b_k$) (peso/peso)	($= b_k/b_l$)
10th percentile	0.00396	0.111	23.3
25th percentile	0.00523	0.139	23.9
50th percentile	0.00579	0.139	24.0
75th percentile	0.00579	0.139	35.3
90th percentile	0.00579	0.260	44.8

Wood (2010)			
	Marginal Productivity		Marginal Rate of Substitution
	Labor ($= b_l$)	Capital ($= b_k$)	($= b_k/b_l$)
10th percentile	1.46×10^{-18}	0.816	760
25th percentile	8.55×10^{-16}	0.816	760
50th percentile	0.00133	1.01	760
75th percentile	0.00133	1.01	9.73×10^{14}
90th percentile	0.00133	1.01	5.59×10^{17}



(a) Plastic (2520)

(b) Wood (2010)

Figure 5. Estimated Production Function.

Table 18. Coefficient of contextual variables.

	Plastic (2520)		Wood (2010)	
	Dummy of exporting	Share of exporting in sales	Dummy of exporting	Share of exporting in sales
Point estimate	334.5	303.7	-763.0	4114
95% lower bound	148.7	-334.3	-1944	2568
95% upper bound	520.3	941.8	417.7	5660
p -value	4.70×10^{-4}	0.3493	0.2033	5.64×10^{-7}

added output is the largest for establishments with high capital to labor ratios indicating capital intensive establishments have increased actual output. Furthermore, labor intensive establishments have smaller most productive scale size in both industries. This is consistent with the theory of the firm in which firms grow and become more capital intensive over time by automating processes with capital and using less labor.

Table 19. Most Productive Scale Size for each Capital/Labor ratio.

Plastic (2520)			
Capital/Labor percentile	MPSS Labor	MPSS Capital	Output (Value added)
10th percentile	619580	519.1	3290
25th percentile	529980	1344	3010
50th percentile	529980	2604	3185
75th percentile	529980	5617	3602
90th percentile	529980	10270	4248
Wood (2010)			
Capital/Labor percentile	MPSS Labor	MPSS Capital	Output (Value added)
10th percentile	2531100	741.6	1659
25th percentile	1045000	1200	2142
50th percentile	867250	2712	3470
75th percentile	662700	4179	4682
90th percentile	458150	5644	5893

8 Conclusion

This paper proposed SCKLS that imposes shape constraints on a local polynomial estimator. We show the consistency and convergence rate of this new estimator, as well as its relationship with CNLS and CWB. We also illustrate how to use SCKLS to validate the imposed shape constraints, and to test whether a function is affine. In applications where out-of-sample performance is less critical and the boundary behavior is of less concern, such as regulation applications, the CNLS estimator might be preferred due to its simplicity. In contrast, the case where out-of-sample performance is important, such as survey data, the SCKLS estimator is more robust. Simulation results reveal the SCKLS estimator outperforms existing estimators CNLS and CWB in most scenarios. In addition, we validate the usefulness of several extensions, including variable bandwidth and non-uniform gridding, are important to estimate function with non-uniform input data set which is common in

manufacturing survey and census data. Finally, we demonstrate the SCKLS estimator empirically using Chilean manufacturing data. We compute marginal productivity, marginal rate of substitution, most productive scale size and the effects of exporting, and provide several economic insights to the Chilean plastic and wood manufacturing.

One of the limitations of SCKLS estimator is its computation efficiency due to the large number of constraints. The algorithm we proposed for reducing constraints performs well, and we demonstrate the ability to solve large problems instances within a reasonable time periods. Furthermore, our simulation results show good functional estimates even with a rough grid. Consequently, we can make use of the flexibility of the evaluation points to reduce the computational time of the estimator.

Potential future research could focus on the bandwidth selection methods. Typically, optimal bandwidth selection methods without shape constraints try to trade bias and variance to find the best estimator in terms of RMSE. Since the imposed shape restrictions already constrain the variance of the estimator to some extent, we expect that the optimal bandwidth in the SCKLS estimator will be smaller than the optimal unconstrained estimator. Further, if systematic inefficiency is present in the data, deconvoluting the residuals following the stochastic frontier literature would allow the investigation of a production frontier.

SUPPLEMENTARY MATERIAL

Appendix: The document contains: (A) extensions to the CWB estimator; (B) comparison between piece-wise linear and smooth estimates; (C) technical proofs of the theoretical results; (D) an algorithm for SCKLS computational performance; (E) comprehensive results of existing and additional numerical experiments; and (F) semi-parametric model to integrate contextual variable.

MATLAB code: MATLAB code to compute SCKLS estimator described in the article. The package also contains some examples.

Appendix

A Extensions to the CWB estimator and the relationship between SCKLS, CWB and CNLS

A.1 Calculating the first partial derivative of $\hat{g}(\mathbf{x}|\mathbf{p})$ for CWB

Du et al. (2013) proposed the CWB estimator which requires estimating the first partial derivatives of unconstrained functional estimates, $\hat{g}^{(1)}(\mathbf{x}|\mathbf{p})$. Here, we test two different methods to calculate the partial derivative. The first method is to calculate numerical derivative, $\hat{g}^{(1)}(\mathbf{x}|\mathbf{p}) = \frac{\hat{g}(\mathbf{x}+\Delta|\mathbf{p})-\hat{g}(\mathbf{x}|\mathbf{p})}{\Delta}$, to obtain the approximated derivative estimate. Racine (2016) shows that the numerical derivative is very close to the analytic derivative. The second method is to use the slope estimates of local linear estimator directly as a proxy for the first partial derivative. We evaluate the performance of CWB in p -space estimator with these two different methods. Table A.1 and A.2 summarize the RMSE performance against the true function on observed points and evaluation points respectively. The experimental setting is based on Experiment 1 in Section 5.1.

Table A.1. RMSE on observation points for different methods to obtain $\hat{g}^{(1)}(\mathbf{x}|\mathbf{p})$.

Number of observations		Average RMSE on observation points				
		100	200	300	400	500
2-input	Numerical derivative	0.260	0.163	0.143	0.153	0.164
	Slope estimates of LL	0.421	0.357	0.284	0.306	0.293
3-input	Numerical derivative	0.236	0.256	0.208	0.246	0.240
	Slope estimates of LL	0.356	0.427	0.336	0.294	0.279
4-input	Numerical derivative	0.259	0.226	0.222	0.216	0.210
	Slope estimates of LL	0.388	0.397	0.276	0.261	0.259

The results show that the CWB estimator using the numerical derivative performances better than CWB using the slope estimates from the local linear kernel estimator particularly when the sample size is small. A plausible reason for this result is that the rate of convergence of slope estimates in local linear estimator are slower than that of functional estimates, i.e., slope estimates are not very accurate when the dataset is small. In contrast, the numerical derivative uses the functional estimate to calculate the partial derivative

Table A.2. RMSE on evaluation points for different methods to obtain $\hat{g}^{(1)}(\mathbf{x}|\mathbf{p})$.

Number of observations		Average RMSE on evaluation points				
		100	200	300	400	500
2-input	Numerical derivative	0.284	0.188	0.157	0.176	0.193
	Slope estimates of LL	0.445	0.387	0.321	0.334	0.323
3-input	Numerical derivative	0.309	0.355	0.272	0.331	0.271
	Slope estimates of LL	0.438	0.507	0.403	0.371	0.363
4-input	Numerical derivative	0.408	0.381	0.354	0.333	0.308
	Slope estimates of LL	0.530	0.535	0.396	0.387	0.368

of $\hat{g}(\mathbf{x}|\mathbf{p})$. Consequently, the numerical derivative does not suffer from the slow rate of convergent of slope estimates of the local linear kernel.

A.2 CWB estimator that minimize the distance from the observed data

Since the objective function of the CWB estimator potentially pulls the functional estimate away from the true function and towards the unrestricted estimate, the CWB estimator may suffer from a finite sample bias. To avoid this problem, we propose an extension of the CWB estimator by converting the objective function from p -space to y -space. Instead of minimizing the distance between the unconstrained estimator and the shape restricted functional estimate by minimizing the distance between the two functions in p -space, we propose minimizing the distance between the observed vector of y and the shape restricted functional estimate in y -space. The estimator is formulated as follows:

$$\begin{aligned}
 \min_{\mathbf{p}} \quad & D_y(\mathbf{p}) = \sum_{j=1}^n (y_j - \hat{g}(\mathbf{X}_j|\mathbf{p}))^2 \\
 \text{subject to} \quad & l(\mathbf{x}_i) \leq \hat{g}^{(s)}(\mathbf{x}_i|\mathbf{p}) \leq u(\mathbf{x}_i), \quad i = 1, \dots, m \\
 & \sum_{j=1}^n p_j = 1
 \end{aligned} \tag{A.1}$$

Since the objective function is not necessarily convex in \mathbf{p} , this problem is a general nonlinear optimization problem which is hard to solve. In appendix A.3, we show the relationship between our alternative, which we will refer to as CWB in y -space, and Shape Constrained Kernel-weighted Least Squares (SCKLS).

A.3 The relationship between SCKLS, CWB and CNLS

We describe the relationship of CWB and SCKLS. To begin with, note the concavity and monotonicity constraint in (6) are just examples of the more general constraints in either CWB in p -space (3) or in y -space (A.1). Comparing the objective function of CWB in y -space (A.1) and SCKLS (6), the SCKLS estimator is obtained by minimizing the weighted sum of squared residuals, while the CWB estimator in y -space is obtained by minimizing the sum of squared residuals. Namely, the kernel weight is used to weight the sum of squared residuals in the SCKLS estimator while it is used to weight each observation to obtain functional estimate in the CWB estimator in y -space.

To describe further the relationship between the CWB estimator in y -space and SCKLS we focus on the special case of SCKLS when the bandwidth vector goes to zero (i.e. CNLS). First notice CNLS and CWB in y -space have the same sum of squared residuals objective function. The only difference between CNLS and the CWB estimator in y -space is the form of the functional and slope estimates which is summarized at Table A.3. The CNLS estimator defines the functional and slope estimates as decision variables of the optimization problem. In contrast, the CWB estimator in y -space defines the functional and slope estimates as consisting of two parts: the unrestricted local weighting estimator and observation specific weights. This decomposition allows a smooth functional estimate, but potentially leads to a non-convex objective function increasing the computational difficulty of the optimization problem. Further, this decomposition can introduce a finite sample bias because the estimate depends on the unrestricted local weighting estimates which are not necessarily close to the true function in the case of finite sample.

Table A.3. Expression of functional and slope estimates.

	CNLS	CWB in y -space
Functional estimates ($= \hat{g}(\mathbf{X}_j)$)	$\hat{y}_j = \hat{\alpha}_j + \hat{\beta}'_j \mathbf{X}_j$	$\sum_{l=1}^n \hat{p}_l \cdot A_l(\mathbf{X}_j) y_l$
Slope estimates ($= \frac{\partial \hat{g}}{\partial \mathbf{x}}(\mathbf{X}_j)$)	$\hat{\beta}_j$	$\sum_{l=1}^n \hat{p}_l \cdot \frac{\partial A_l(\mathbf{X}_j)}{\partial \mathbf{x}} y_l$

B Comparison between piece-wise linear and smooth estimates

The SCKLS estimator is piece-wise linear which approximates a smooth true production function. Piece-wise linear functional estimators are often criticized as a rough approximation. In this section, we show that under monotonicity and concavity constraints, even smooth estimators tend to select approximately piece-wises linear estimates.

We estimate a production function using B-spline with monotonicity and concavity constraints. Recall B-splines is a smooth estimator which would not favor a piece-wise approximation. We impose the monotonicity and concavity on a grid of 50 uniform evaluation points, and use 20 knots to implement a quadratic B-splines estimator. We consider the following DGP: Cobb–Douglas production function with one-input and one-output, $g_0(x) = x^{0.5}$, where observed input X_j is randomly and independently drawn from uniform distribution, $unif[1, 10]$, and the additive noise, ϵ_j , is randomly and independently sampled from a normal distribution, $N(0, 0.5^2)$, and $y_j = g_0(X_j) + \epsilon_j$. Figure A.1 is the graph of the functional estimate of shape constrained B-spline from a typical run. Although both the true function and the estimator are smooth, visually the estimate appears to be a piece-wise linear function composed of three hyperplanes.

C Technical proofs

C.1 Alternative definitions of SCKLS

Recall that given observations $\{\mathbf{X}_j, y_j\}_{j=1}^n$ and evaluation points $\{\mathbf{x}_i\}_{i=1}^m$, the (unconstrained) local linear estimator at \mathbf{x}_i is $(\tilde{a}_i, \tilde{\mathbf{b}}_i)$ for $i = 1, \dots, m$, where $(\tilde{a}_1, \tilde{\mathbf{b}}_1, \dots, \tilde{a}_m, \tilde{\mathbf{b}}_m)$ is the (unique) minimizer of

$$\sum_{i=1}^m \sum_{j=1}^n (y_j - a_i - (\mathbf{X}_j - \mathbf{x}_i)' \mathbf{b}_i)^2 K \left(\frac{\mathbf{X}_j - \mathbf{x}_i}{\mathbf{h}} \right).$$

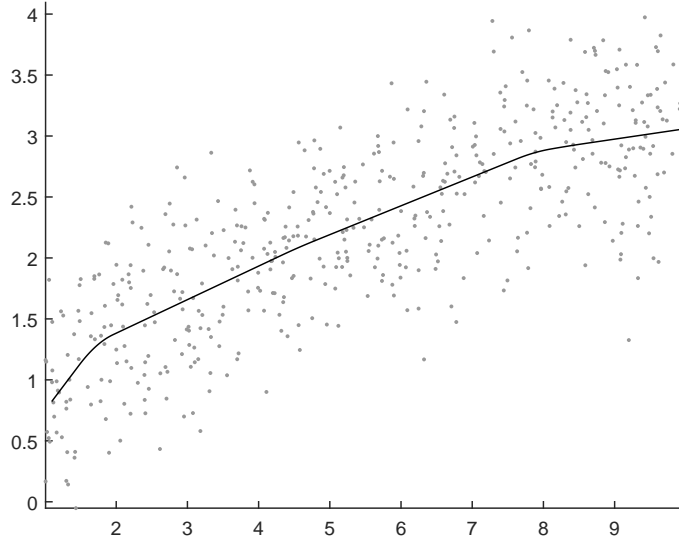


Figure A.1. Functional estimates of Shape Constrained B-spline.

For simplicity, we assume that the bandwidth vector $\mathbf{h} = (h, \dots, h)'$. Since the objective function is quadratic, for any $(a_1, \mathbf{b}_1, \dots, a_m, \mathbf{b}_m)$, its value equals

$$nh^d \sum_{i=1}^m (\tilde{a}_i - a_i, (\tilde{\mathbf{b}}_i - \mathbf{b}_i)'h) \Sigma_i \begin{pmatrix} \tilde{a}_i - a_i \\ (\tilde{\mathbf{b}}_i - \mathbf{b}_i)h \end{pmatrix} + \text{Const}$$

where

$$\Sigma_i = \frac{1}{nh^d} \sum_{j=1}^n U\left(\frac{\mathbf{X}_j - \mathbf{x}_i}{h}\right) \left\{ U\left(\frac{\mathbf{X}_j - \mathbf{x}_i}{h}\right) \right\}' K\left(\frac{\mathbf{X}_j - \mathbf{x}_i}{h}\right)$$

with $U(\mathbf{x})$ being the vector $(1, \mathbf{x}')'$ and

$$\text{Const} = \sum_{i=1}^m \sum_{j=1}^n (y_j - \tilde{a}_i - (\mathbf{X}_j - \mathbf{x}_i)' \tilde{\mathbf{b}}_i)^2 K\left(\frac{\mathbf{X}_j - \mathbf{x}_i}{h}\right).$$

Therefore, SCKLS could be viewed as a minimizer of

$$\sum_{i=1}^m (\tilde{a}_i - a_i, (\tilde{\mathbf{b}}_i - \mathbf{b}_i)'h) \Sigma_i \begin{pmatrix} \tilde{a}_i - a_i \\ (\tilde{\mathbf{b}}_i - \mathbf{b}_i)h \end{pmatrix}$$

subject to the shape constraints imposed on $(a_1, \mathbf{b}_1, \dots, a_m, \mathbf{b}_m)$. More generally, fixing $\{\mathbf{X}_1, \dots, \mathbf{X}_n\}$, $\{\mathbf{x}_1, \dots, \mathbf{x}_m\}$ and h , and define a new squared distance measure between

two functions g_1, g_2 as

$$\|g_1 - g_2\|_{n,m}^2 = \frac{1}{m} \sum_{i=1}^m \left(g_1(\mathbf{x}_i) - g_2(\mathbf{x}_i), \left(\frac{\partial(g_1 - g_2)}{\partial \mathbf{x}}(\mathbf{x}_i) \right)' h \right) \Sigma_i \left(\frac{g_1(\mathbf{x}_i) - g_2(\mathbf{x}_i)}{\frac{\partial(g_1 - g_2)}{\partial \mathbf{x}}(\mathbf{x}_i) h} \right),$$

then SCKLS belongs to

$$\operatorname{argmin}_{g \in G_2} \|g - \tilde{g}_n\|_{n,m}$$

where G_2 is the set that contains all the concave and increasing functions from \mathbf{S} to \mathbb{R} .

Below, we list some useful results on the behaviors of Σ_i and $(\tilde{a}_i, \tilde{\mathbf{b}}_i)$. These results follow from Lemma 5 and 11, and Proposition 7 of Fan and Guerre (2016) respectively.

lemma 1. *Suppose that Assumption 1(i)-1(vi) hold, then with probability one, there exists $C > 1$ such that the eigenvalues of Σ_i are in $[1/C, C]$ for all $i = 1, \dots, m$ for sufficiently large n .*

lemma 2. *Suppose that Assumption 1(i)-1(vi) hold, then*

$$\sup_{i=1, \dots, m} \left(|\tilde{a}_i - g_0(\mathbf{x}_i)|^2, \left\| h \left\{ \tilde{\mathbf{b}}_i - \frac{\partial g_0}{\partial \mathbf{x}}(\mathbf{x}_i) \right\} \right\|^2 \right) = O_p(n^{-4/(4+d)} \log n)$$

for sufficiently large n .

C.2 Proof of Theorems in Section 4

Theorem 1.

1. **(The case of a fixed m)** *Suppose that Assumption 1(i)-1(vi) and Assumption 2(i) hold. Then, as $n \rightarrow \infty$, with probability one, the estimates from SCKLS satisfy*

$$\hat{a}_i \rightarrow g_0(\mathbf{x}_i) \quad \text{and} \quad \hat{\mathbf{b}}_i \rightarrow \frac{\partial g_0}{\partial \mathbf{x}}(\mathbf{x}_i)$$

for all $i = 1, \dots, m$.

2. **(The case of an increasing m)** *Suppose that Assumption 1(i)-1(vi) and Assumption 2(ii) hold. Let \mathbf{C} be any fixed closed set that belongs to the interior of \mathbf{S} . Then with*

probability one, , as $n \rightarrow \infty$, the SCKLS estimator satisfy

$$\sup_{\mathbf{x} \in \mathcal{C}} |\hat{g}_n(\mathbf{x}) - g_0(\mathbf{x})| \rightarrow 0.$$

Proof. The uniqueness of the estimates of \hat{a}_i and $\hat{\mathbf{b}}_i$ is established because our objective function corresponds to is a quadratic programming problem with a positive definite (strictly convex) objective function with a feasible solution. See Bertsekas (1995).

Based on our characterization of SCKLS in Section C.1, we note that the objective function at the SCKLS is smaller than that at the truth, and thus

$$\begin{aligned} & \sum_{i=1}^m (\tilde{a}_i - \hat{a}_i, (\tilde{\mathbf{b}}_i - \hat{\mathbf{b}}_i)'h) \Sigma_i \begin{pmatrix} \tilde{a}_i - \hat{a}_i \\ (\tilde{\mathbf{b}}_i - \hat{\mathbf{b}}_i)h \end{pmatrix} \\ & \leq \sum_{i=1}^m \left(\tilde{a}_i - g_0(\mathbf{x}_i), (\tilde{\mathbf{b}}_i - \frac{\partial g_0}{\partial \mathbf{x}}(\mathbf{x}_i))'h \right) \Sigma_i \begin{pmatrix} \tilde{a}_i - g_0(\mathbf{x}_i) \\ (\tilde{\mathbf{b}}_i - \frac{\partial g_0}{\partial \mathbf{x}}(\mathbf{x}_i))h \end{pmatrix} \end{aligned}$$

For the first claim, we note that in view of Lemma 2, the right hand side of the above inequality is $O_p(n^{-4/(4+d)} \log n)$ as $n \rightarrow \infty$. Moreover, in view of Lemma 1,

$$\frac{1}{C} \sum_{i=1}^m \left[|\tilde{a}_i - \hat{a}_i|^2 + \left\| h(\tilde{\mathbf{b}}_i - \hat{\mathbf{b}}_i) \right\|^2 \right] \leq \sum_{i=1}^m (\tilde{a}_i - \hat{a}_i, (\tilde{\mathbf{b}}_i - \hat{\mathbf{b}}_i)'h) \Sigma_i \begin{pmatrix} \tilde{a}_i - \hat{a}_i \\ (\tilde{\mathbf{b}}_i - \hat{\mathbf{b}}_i)h \end{pmatrix}.$$

It follows that $|\tilde{a}_i - \hat{a}_i| = O_p(n^{-2/(4+d)} \log n) \rightarrow 0$ and $\|\tilde{\mathbf{b}}_i - \hat{\mathbf{b}}_i\| = O_p(n^{-2/(4+d)} \log n) \rightarrow 0$ in probability. Consequently, it follows from Lemma 2 that $\hat{a}_i \rightarrow g(\mathbf{x}_i)$ and $\hat{\mathbf{b}}_i \rightarrow \frac{\partial g}{\partial \mathbf{x}}(\mathbf{x}_i)$ for all i , thus the first claim is proved.

Now for the second claim, we note that it follows from Lemma 1 and Lemma 2 that

$$\begin{aligned} \frac{1}{Cm} \sum_{i=1}^m (\tilde{a}_i - \hat{a}_i)^2 & \leq \frac{1}{m} \sum_{i=1}^m (\tilde{a}_i - \hat{a}_i, (\tilde{\mathbf{b}}_i - \hat{\mathbf{b}}_i)'h) \Sigma_i \begin{pmatrix} \tilde{a}_i - \hat{a}_i \\ (\tilde{\mathbf{b}}_i - \hat{\mathbf{b}}_i)h \end{pmatrix} \\ & \leq \frac{1}{m} \sum_{i=1}^m \left(\tilde{a}_i - g_0(\mathbf{x}_i), (\tilde{\mathbf{b}}_i - \frac{\partial g_0}{\partial \mathbf{x}}(\mathbf{x}_i))'h \right) \Sigma_i \begin{pmatrix} \tilde{a}_i - g_0(\mathbf{x}_i) \\ (\tilde{\mathbf{b}}_i - \frac{\partial g_0}{\partial \mathbf{x}}(\mathbf{x}_i))h \end{pmatrix} = o_p(1) \end{aligned}$$

as $n \rightarrow \infty$. For mathematical convenience, the last line above can be temporarily strengthened to almost surely convergence using the Skorokhod's representation device.

Suppose that given the number of observations j , the corresponding SCKLS is \hat{g}_j . By

Theorem 10.9 of Rockafellar (1970), it is possible to select a subsequence of any subsequence of $\{\hat{g}_j\}_j$ such that it converges uniformly on \mathbf{C} to g^* , a closed subset of the interior of \mathbf{S} . Note that g^* must be g_0 on \mathbf{C} , because otherwise, there exists a non-degenerate region $\mathbf{S}^* \subset \mathbf{S}$ such that $\inf_{\mathbf{x} \in \mathbf{S}^*} |g^*(\mathbf{x}) - g_0(\mathbf{x})| > \epsilon$ for some $\epsilon > 0$, and thus

$$\frac{1}{m} \sum_{i=1}^m (\tilde{a}_i - \hat{a}_i)^2 \geq \frac{1}{m} \sum_{i=1}^m (\tilde{a}_i - \hat{a}_i)^2 \mathbf{1}_{\{\mathbf{x}_i \in \mathbf{S}^*\}}$$

which in the limit is $\geq \epsilon^2 P(\mathbf{x}_i \in \mathbf{S}^*) > 0$, leading to a contradiction.

Consequently, because every subsequence of $\{\hat{g}_j\}_j$ has a further subsequence that converges to g_0 on \mathbf{C} , $\{\hat{g}_j\}_j$ converges to g_0 on \mathbf{C} , as $n \rightarrow \infty$. \square

Theorem 2. *Suppose that Assumption 1(i)-1(vi) and Assumption 2(i) or 2(ii) hold. Then,*

$$\frac{1}{m} \sum_{i=1}^m \{\hat{g}_n(\mathbf{x}_i) - g_0(\mathbf{x}_i)\}^2 = O(n^{-4/(4+d)} \log n)$$

Proof. Let \tilde{a}_i and \hat{a}_i be defined as in the proof of Theorem 1. Note that $\hat{g}_n(\mathbf{x}_i) = \hat{a}_i$. As shown previously, $\frac{1}{m} \sum_{i=1}^m (\tilde{a}_i - \hat{a}_i)^2 = O_p(n^{-4/(4+d)} \log n)$. Also, it follows from Lemma 2 that $\frac{1}{m} \sum_{i=1}^m (\tilde{a}_i - g_0(\mathbf{x}_i))^2 = O_p(n^{-4/(4+d)} \log n)$. Consequently,

$$\frac{1}{m} \sum_{i=1}^m (\hat{g}_n(\mathbf{x}_i) - g_0(\mathbf{x}_i))^2 \leq \frac{2}{m} \sum_{i=1}^m (\tilde{a}_i - \hat{a}_i)^2 + \frac{2}{m} \sum_{i=1}^m (\tilde{a}_i - g_0(\mathbf{x}_i))^2 = O_p(n^{-4/(4+d)} \log n).$$

\square

Theorem 3. *Suppose that Assumption 1(i)-1(vi), Assumption 2(ii) and Assumption 3 hold. Then, with probability one, as $n \rightarrow \infty$, the SCKLS estimator satisfies*

$$\sup_{\mathbf{x} \in \mathbf{S}} |\hat{g}_n(\mathbf{x}) - g_0(\mathbf{x})| \rightarrow 0.$$

Proof. It follows from Theorem 2 that

$$\sum_{i=1}^m (\hat{g}_n(\mathbf{x}_i) - g_0(\mathbf{x}_i))^2 = O_p(mn^{-4/(4+d)} \log n) = o_p(1).$$

Similarly, using the arguments demonstrated in the proofs of Theorem 1 and Theorem 2,

we can show that

$$\sum_{i=1}^m \left\| \frac{\partial \hat{g}_n(\mathbf{x}_i)}{\partial \mathbf{x}} - \frac{\partial g_0(\mathbf{x}_i)}{\partial \mathbf{x}} \right\|^2 = O_p(h^{-2} m n^{-4/(4+d)} \log n) = O_p(1).$$

These imply that $\max_{i=1, \dots, m} |\hat{g}_n(\mathbf{x}_i)| = O_p(1)$ and $\max_{i=1, \dots, m} \left\| \frac{\partial \hat{g}_n(\mathbf{x}_i)}{\partial \mathbf{x}} \right\|_{\infty} = O_p(1)$. Since

$$\hat{g}_n(\mathbf{x}) = \min_{i \in \{1, \dots, m\}} \left\{ \hat{g}_n(\mathbf{x}_i) + (\mathbf{x} - \mathbf{x}_i)' \frac{\partial \hat{g}_n(\mathbf{x}_i)}{\partial \mathbf{x}} \right\},$$

we have that

$$\sup_{\mathbf{x} \in \mathcal{S}} |\hat{g}_n(\mathbf{x})| = O_p(1) \quad \text{and} \quad \sup_{\mathbf{x} \in \mathcal{S}} \left\| \frac{\partial \hat{g}_n(\mathbf{x})}{\partial \mathbf{x}} \right\|_{\infty} = O_p(1).$$

These findings, combined with Theorem 1, yield the consistency of \hat{g}_n over \mathcal{S} .

□

Theorem 4. *Suppose that Assumption 1(v) and Assumption 4 holds. Then, for any n , when the vector of bandwidth approaches zero, i.e. $\|\mathbf{h}\| \rightarrow \mathbf{0}$ (where $\mathbf{h} = (h_1, \dots, h_d)'$) the SCKLS estimator \hat{g}_n converges to the CNLS estimator \tilde{g}_n pointwise at $\mathbf{X}_1, \dots, \mathbf{X}_n$.*

Proof. In view of Assumption 1(v), for any sufficiently small \mathbf{h} , we have

$$K\left(\frac{\mathbf{X}_j - \mathbf{x}_i}{\mathbf{h}}\right) = \begin{cases} 0 & \text{if } \mathbf{x}_i \neq \mathbf{X}_j, \\ K(\mathbf{0}) & \text{if } \mathbf{x}_i = \mathbf{X}_j, \end{cases} \quad \text{for } \forall i, j.$$

Then, the objective function of (6) is equal to $\sum_{j=1}^n (y_j - a_j)^2 K(\mathbf{0})$, and thus

$$\operatorname{argmin}_{a_j, \mathbf{b}_j} \sum_{j=1}^n (y_j - a_j)^2 K(\mathbf{0}) = \operatorname{argmin}_{a_j, \mathbf{b}_j} \sum_{j=1}^n (y_j - a_j)^2$$

Writing $a_j = \alpha_j + \beta_j' \mathbf{X}_j$ and $\mathbf{b}_j = \beta_j$ for $j = 1, \dots, n$ by definition. Then, quadratic

programming problem (6) can be rewritten as follows:

$$\begin{aligned} \min_{\alpha, \beta} \quad & \sum_{j=1}^n (y_j - (\alpha_j + \beta_j' \mathbf{X}_j))^2 \\ \text{subject to} \quad & \alpha_j + \beta_j' \mathbf{X}_j \leq \alpha_l + \beta_l' \mathbf{X}_j, \quad j, l = 1, \dots, n \\ & \beta_j \geq 0, \quad j = 1, \dots, n \end{aligned}$$

which is equivalent to the formulation of the CNLS estimator (1). \square

Theorem 5. *Given Assumption 1(v). For any given n , when the bandwidth approaches to infinity, the SCKLS estimator converges to the least squares estimator of the linear regression model subject to monotonicity constraints.*

Proof. When $\mathbf{h} \rightarrow \infty$, we have

$$K\left(\frac{\mathbf{X}_j - \mathbf{x}_i}{\mathbf{h}}\right) = K(\mathbf{0}) \quad \text{for } \forall i, j. \quad (\text{A.2})$$

By substituting (A.2) into the objective function of (6) converges to

$$\sum_{i=1}^m \sum_{j=1}^n (y_j - a_i - (\mathbf{X}_j - \mathbf{x}_i)' \mathbf{b}_i)^2 K(\mathbf{0}).$$

Next, we derived the minimum of the objective function in the limit. Let's consider

$$\operatorname{argmin}_{a_i, \mathbf{b}_i} \sum_{i=1}^m \sum_{j=1}^n (y_j - a_i - (\mathbf{X}_j - \mathbf{x}_i)' \mathbf{b}_i)^2 \quad (\text{A.3})$$

subject to constraints. Rewrite $a_i + (\mathbf{X}_j - \mathbf{x}_i)' \mathbf{b}_i = \alpha_i + \beta_i' \mathbf{X}_j$ for $i = 1, \dots, m$ and $j = 1, \dots, n$. Then the objective function of (6) can be rewritten as follows with (A.3).

$$\begin{aligned} \min_{\alpha_i, \beta_i} \quad & \sum_{i=1}^m \sum_{j=1}^n (y_j - (\alpha_i + \beta_i' \mathbf{X}_j))^2 \\ \text{subject to} \quad & \alpha_i + \beta_i' \mathbf{x}_i \leq \alpha_l + \beta_l' \mathbf{x}_i \quad i, l = 1, \dots, m \\ & \beta_i \geq 0 \quad i = 1, \dots, m \end{aligned}$$

Here, since we do not impose any weight on the objective function, it is easy to see that

$\alpha_1 = \dots = \alpha_m$ and $\beta_1 = \dots = \beta_m$. Then the Afriat constraints become redundant, resulting in

$$\begin{aligned} \min_{\alpha, \beta} \quad & \sum_{j=1}^n (y_j - (\alpha + \beta' \mathbf{X}_j))^2 \\ \text{subject to} \quad & \beta \geq 0. \end{aligned}$$

It remains to show that as $\mathbf{h} \rightarrow \mathbf{0}$, the minimum of objective function of (6) for each \mathbf{h} also converges to the minimum of the objective function in the limit (with $\mathbf{h} = \mathbf{0}$). This is indeed the case because the objective function is quadratic (both for any \mathbf{h} and in the limit when $\mathbf{h} \rightarrow \mathbf{0}$).

□

C.3 Proof of Theorems in Section 5

When developing the test for an affine function in Section 5, the estimators \hat{g}_n^V and \hat{g}_n^Λ are defined. Where \hat{g}_n^V is the SCKLS estimator using only a set of convexity constraints, while \hat{g}_n^Λ is the SCKLS estimator using only a set of concavity constraints. Below we explicitly formulate these mathematical programs. First, \hat{g}_n^V , the SCKLS estimator with only a set of convexity constraints is defined as

$$\begin{aligned} \min_{a_i, \mathbf{b}_i} \quad & \sum_{i=1}^m \sum_{j=1}^n (y_j - a_i - (\mathbf{X}_j - \mathbf{x}_i)' \mathbf{b}_i)^2 K \left(\frac{\mathbf{X}_j - \mathbf{x}_i}{\mathbf{h}} \right) \\ \text{subject to} \quad & a_i - a_l \leq \mathbf{b}_i' (\mathbf{x}_i - \mathbf{x}_l), \quad i, l = 1, \dots, m \end{aligned}$$

Furthermore, \hat{g}_n^Λ , the SCKLS estimator using only a set of concavity constraints is defined as

$$\begin{aligned} \min_{a_i, \mathbf{b}_i} \quad & \sum_{i=1}^m \sum_{j=1}^n (y_j - a_i - (\mathbf{X}_j - \mathbf{x}_i)' \mathbf{b}_i)^2 K \left(\frac{\mathbf{X}_j - \mathbf{x}_i}{\mathbf{h}} \right) \\ \text{subject to} \quad & a_i - a_l \geq \mathbf{b}_i' (\mathbf{x}_i - \mathbf{x}_l), \quad i, l = 1, \dots, m \end{aligned}$$

These will be used in Theorem 7 later.

Theorem 6. *Suppose that Assumption 1(i),(ii),(iv)–(vi) and Assumption 2(ii) hold. Furthermore, assume that g_0 is twice-differentiable. Then, our test is consistent, i.e., under*

H_1 , for any $\alpha \in (0, 1)$, the probability of rejecting H_0 tends to 1 as $B \rightarrow \infty$ and $n \rightarrow \infty$.

Proof. First, we show that there exists some $c_1 > 0$ such that $T_n > c_1$ with probability one as $n \rightarrow \infty$. Let \mathbf{S}' be a closed subset of $\text{int}(\mathbf{S})$ such that $g_0 \notin G_2$ on \mathbf{S}' . Note that

$$\begin{aligned} T_n &= \frac{1}{m} \sum_{i=1}^m \{\hat{g}_n(\mathbf{x}_i) - \tilde{g}_n(\mathbf{x}_i)\}^2 \geq \inf_{g \in G_2} \frac{1}{m} \sum_{i=1}^m \{g(\mathbf{x}_i) - \tilde{g}_n(\mathbf{x}_i)\}^2 \\ &\geq \frac{1}{m} \sum_{i=1}^m \{\hat{g}_n^{CNLS-LL}(\mathbf{x}_i) - \tilde{g}_n(\mathbf{x}_i)\}^2 \mathbf{1}_{\{\mathbf{x}_i \in \mathbf{S}'\}}, \end{aligned}$$

where $\hat{g}_n^{CNLS-LL} \in \text{argmin}_{g \in G_2} \frac{1}{m} \sum_{i=1}^m \{g(\mathbf{x}_i) - \tilde{g}_n(\mathbf{x}_i)\}^2$.

Using the argument in Proposition 4 and the proof of Theorem 1 (i.e. Step 5) of Lim and Glynn (2012), we can show that there exists some constant $c_2 > 0$ such that for sufficient large n , $\sup_{\mathbf{x} \in \mathbf{S}'} |\hat{g}_n^{CNLS-LL}(\mathbf{x})| < c_2$ and $\hat{g}_n^{CNLS-LL}$ is Lipschitz over \mathbf{S}' uniformly in n . Furthermore, it follows from Theorem 10.9 of Rockafellar (1970) that for any subsequence of $\{\hat{g}_{n(k)}^{CNLS-LL}\}$, there exists a further subsequence $\{\hat{g}_{n(k_l)}^{CNLS-LL}\}$ that converges to some g^* pointwise in \mathbf{S}' . Let Q_n be the empirical distribution of $\{\mathbf{x}_1, \dots, \mathbf{x}_m\}$ (here m depends on n and $Q_n \xrightarrow{d} Q$). We now have that

$$\liminf_{n \rightarrow \infty} \frac{1}{m} \sum_{i=1}^m \{\hat{g}_n^{CNLS-LL}(\mathbf{x}_i) - \tilde{g}_n(\mathbf{x}_i)\}^2 \mathbf{1}_{\{\mathbf{x}_i \in \mathbf{S}'\}} = \liminf_{n \rightarrow \infty} \int_{\mathbf{S}} \{\hat{g}_n^{CNLS-LL}(\mathbf{x}) - \tilde{g}_n(\mathbf{x})\}^2 \mathbf{1}_{\{\mathbf{x} \in \mathbf{S}'\}} Q_n(d\mathbf{x}).$$

By picking suitable subsequences, we could rewrite the right hand side of above as

$$\begin{aligned} &\lim_{k \rightarrow \infty} \int_{\mathbf{S}} \{\hat{g}_{n(k)}^{CNLS-LL}(\mathbf{x}) - \tilde{g}_{n(k)}(\mathbf{x})\}^2 \mathbf{1}_{\{\mathbf{x} \in \mathbf{S}'\}} Q_{n(k)}(d\mathbf{x}) \\ &= \lim_{l \rightarrow \infty} \int_{\mathbf{S}} \{\hat{g}_{n(k_l)}^{CNLS-LL}(\mathbf{x}) - \tilde{g}_{n(k_l)}(\mathbf{x})\}^2 \mathbf{1}_{\{\mathbf{x} \in \mathbf{S}'\}} Q_{n(k_l)}(d\mathbf{x}) \\ &= \lim_{l \rightarrow \infty} \int_{\mathbf{S}} \{\hat{g}_{n(k_l)}^{CNLS-LL}(\mathbf{x}) - \tilde{g}_{n(k_l)}(\mathbf{x})\}^2 \mathbf{1}_{\{\mathbf{x} \in \mathbf{S}'\}} Q(d\mathbf{x}) \\ &\quad + \lim_{l \rightarrow \infty} \int_{\mathbf{S}} \{\hat{g}_{n(k_l)}^{CNLS-LL}(\mathbf{x}) - \tilde{g}_{n(k_l)}(\mathbf{x})\}^2 \mathbf{1}_{\{\mathbf{x} \in \mathbf{S}'\}} (Q_{n(k_l)} - Q)(d\mathbf{x}) \end{aligned}$$

By the dominated convergence theorem, the first term converges to $\int_{\mathbf{S}'} \{g^*(\mathbf{x}) - g_0(\mathbf{x})\}^2 Q(d\mathbf{x})$. In addition, the second term converges to zero due to the Glivenko–Cantelli theorem (a.k.a. uniform law of large numbers). In particular, we also used that fact that both $\hat{g}_{n(k_l)}^{CNLS-LL}$

and $\tilde{g}_{n(k_l)}$ are Lipschitz over \mathbf{S}' uniformly in l , so the set of functions on \mathbf{S}' containing $(\hat{g}_{n(k_l)}^{CNLS-LL} - \tilde{g}_{n(k_l)})^2(\cdot)$ satisfies the entropy condition as required. For more details, see for example van der Vaart and Wellner (1996).

Since $g_0 \notin G_2$ on \mathbf{S}' , $\int_{\mathbf{S}'} \{g^*(\mathbf{x}) - g_0(\mathbf{x})\}^2 Q(d\mathbf{x}) \geq \inf_{g \in G_2} \int_{\mathbf{S}'} \{g(\mathbf{x}) - g_0(\mathbf{x})\}^2 Q(d\mathbf{x}) > 0$. Consequently, there exists some $c_1 > 0$ such that $T_n > c_1$ with probability one as $n \rightarrow \infty$.

Second, $T_{nk} = o_p(1)$. This follows immediately from Proposition 7 of Fan and Guerre (2016) and the fact that both $\tilde{g}_n \rightarrow g_0$ and $\tilde{g}'_n \rightarrow g'_0$ uniformly.

Finally, write $W_{nk} = \mathbf{1}_{\{T_{nk} > c_1/2\}}$. We note that W_{n1}, \dots, W_{nB} are exchangeable. Thus, for any $\alpha \in (0, 1)$, as $n \rightarrow \infty$,

$$\begin{aligned} P(\text{Do not reject } H_0) &= P\left(\frac{1}{B} \sum_{k=1}^B \mathbf{1}_{\{T_n > T_{nk}\}} \leq 1 - \alpha\right) \\ &\leq P(T_n \leq c_1/2) + P\left(\frac{1}{B} \sum_{k=1}^B W_{nk} \geq 1 - \alpha\right) \\ &\leq P(T_n \leq c_1/2) + \frac{E(W_{n1})}{1 - \alpha} \rightarrow 0. \end{aligned}$$

So the power at any alternative converges to 1. \square

Theorem 7. *Suppose that Assumption 1(i),(ii),(iv)–(vi) and Assumption 2(ii) hold. Furthermore, assume that g_0 is twice-differentiable and the error distribution Z is known. Then for any $\alpha \in (0, 1)$, as $n \rightarrow \infty$ and $B \rightarrow \infty$,*

1. *if H_0 is true, then $P(p_n < \alpha) \rightarrow \alpha$;*
2. *if H_0 is false, then $P(p_n < \alpha) \rightarrow 1$.*

In other words, the test is approximately at most size α and is consistent.

Proof. First, we show that under H_0 , the conditional distribution of $T_n | \{\mathbf{X}_1, \dots, \mathbf{X}_n\}$ and $T_{nk} | \{\mathbf{X}_1, \dots, \mathbf{X}_n\}$ are the same. It is easy to see from the objective function (6) that \hat{g}_n^Λ is invariant to affine transformation, i.e., \hat{g}_n^Λ based on $\{\mathbf{X}_j, y_j\}_{j=1}^n$, denoted by $\hat{g}_n^\Lambda(\mathbf{x}; \{\mathbf{X}_j, y_j\}_{j=1}^n)$, satisfies

$$\hat{g}_n^\Lambda(\mathbf{x}; \{\mathbf{X}_j, y_j\}_{j=1}^n) + \beta' \mathbf{x} + \alpha = \hat{g}_n^\Lambda(\mathbf{x}; \{\mathbf{X}_j, y_j + \beta' \mathbf{X}_j + \alpha\}_{j=1}^n)$$

for any $\alpha \in \mathbb{R}$ and $\beta \in \mathbb{R}^d$. The same is also true for \hat{g}_n^V and g_n^L . Therefore, T_n based on $\{\mathbf{X}_j, y_j\}_{j=1}^n$ and $\{\mathbf{X}_j, \epsilon_j\}_{j=1}^n$ are exactly the same, so is the conditional distribution of $T_n|\{\mathbf{X}_1, \dots, \mathbf{X}_n\}$ and $T_{nk}|\{\mathbf{X}_1, \dots, \mathbf{X}_n\}$. Given $\{\mathbf{X}_1, \dots, \mathbf{X}_n\}$, T_{n1}, \dots, T_{nk} are exchangeable, and thus $P(p_n < \alpha|\mathbf{X}_1, \dots, \mathbf{X}_n) = (\lceil \alpha(B+1) \rceil - 1)/(B+1)$. Consequently,

$$P(p_n < \alpha) = E[P(p_n < \alpha|\mathbf{X}_1, \dots, \mathbf{X}_n)] \rightarrow \alpha$$

as $B \rightarrow \infty$.

In addition, under H_0 , it follows from our Theorem 2 and the well-known property of the OLS of linear regression that

$$\frac{1}{m} \sum_{i=1}^m \{\hat{g}_n^\Lambda(\mathbf{x}_i) - g_n^L(\mathbf{x}_i)\}^2 \leq \frac{2}{m} \sum_{i=1}^m \{\hat{g}_n^\Lambda(\mathbf{x}_i) - g_0(\mathbf{x}_i)\}^2 + \frac{2}{m} \sum_{i=1}^m \{g_n^L(\mathbf{x}_i) - g_0(\mathbf{x}_i)\}^2 = o_p(1)$$

as $n \rightarrow \infty$. Since a similar result also holds for $\hat{g}_n^V(\mathbf{x}_i)$, we have that $T_n = o_p(1)$. Furthermore, by construction, T_{nk} both under H_0 and H_1 is also $o_p(1)$.

Second, we define the concave L_2 projection of g_0 with respect to the density function f as

$$g_0^\Lambda = \operatorname{argmin}_{g \in \text{CONCAVE}} \int_{\mathbf{S}} (g_0(\mathbf{x}) - g(\mathbf{x}))^2 q(\mathbf{x}) d\mathbf{x}$$

where the minimization is over all concave functions from \mathbf{S} to \mathbb{R} . The convex L_2 projection of g_0 , denoted as g_0^V , and the affine projection of g_0 , denoted as g_0^L can be defined similarly. It then follows from the proof of Theorem 9 of Sen and Meyer (2017) that under H_1 , at least one of g_0^Λ and g_0^V is not affine (almost everywhere on \mathbf{S}). Without loss of generality, we assume that g_0^V is not affine in the rest of the proof. Mathematically, this means that

$$\int_{\mathbf{S}} (g_0(\mathbf{x}) - g_0^V(\mathbf{x}))^2 q(\mathbf{x}) d\mathbf{x} < \int_{\mathbf{S}} (g_0(\mathbf{x}) - g_0^L(\mathbf{x}))^2 q(\mathbf{x}) d\mathbf{x}.$$

Furthermore, as g_0 is differentiable, we could pick a closed subset of $\text{int}(\mathbf{S})$, denoted as \mathbf{S}' such that

$$\int_{\mathbf{S}} (g_0(\mathbf{x}) - g_0^V(\mathbf{x}))^2 q(\mathbf{x}) d\mathbf{x} < \int_{\mathbf{S}'} (g_0(\mathbf{x}) - g_0^L(\mathbf{x}))^2 q(\mathbf{x}) d\mathbf{x}.$$

To facilitate further investigation of the behavior of T_n under H_1 , we define the following

truncated versions of the ℓ_2 distance, and the distance measure $\|\cdot\|_{n,m}$ given in Section C.1: for any function g_1 and g_2 ,

$$\|g_1 - g_2\|_{2,\mathbf{S}'}^2 = \frac{1}{m} \sum_{i=1}^m (g_1(\mathbf{x}_i) - g_2(\mathbf{x}_i))^2 \mathbf{1}_{\{\mathbf{x}_i \in \mathbf{S}'\}}$$

and

$$\|g_1 - g_2\|_{n,m,\mathbf{S}'}^2 = \frac{1}{m} \sum_{i=1}^m \left(g_1(\mathbf{x}_i) - g_2(\mathbf{x}_i), \left(\frac{\partial(g_1 - g_2)}{\partial \mathbf{x}}(\mathbf{x}_i) \right)' h \right) \Sigma_i \left(\frac{g_1(\mathbf{x}_i) - g_2(\mathbf{x}_i)}{\frac{\partial(g_1 - g_2)}{\partial \mathbf{x}}(\mathbf{x}_i) h} \right) \mathbf{1}_{\{\mathbf{x}_i \in \mathbf{S}'\}}.$$

Similar to what we argued in the proof of Theorem 6, we can show that with arbitrarily high probability, \hat{g}_n^V is bounded and Lipschitz over \mathbf{S}' (with the same constants) for all sufficiently large n . This implies that as $n \rightarrow \infty$ (and so $h \rightarrow 0$), for any arbitrarily small $\epsilon > 0$,

$$\begin{aligned} \|\hat{g}_n^V - \tilde{g}_n\|_{n,m} &\geq \|\hat{g}_n^V - \tilde{g}_n\|_{n,m,\mathbf{S}'} \rightarrow \|\hat{g}_n^V - \tilde{g}_n\|_{2,\mathbf{S}'} \\ &\geq \|\tilde{g}_n - g_n^L\|_{2,\mathbf{S}'} - \|\hat{g}_n^V - g_n^L\|_{2,\mathbf{S}'} \\ &\geq \left\{ \int_{\mathbf{S}'} (g_0(\mathbf{x}) - g_0^L(\mathbf{x}))^2 f(\mathbf{x}) d\mathbf{x} \right\}^{1/2} - \|\hat{g}_n^V - g_n^L\|_{2,\mathbf{S}}. \end{aligned}$$

Here we also used Lemma 1 and Lemma 2 in deriving the above inequalities. On the other hand,

$$\|\hat{g}_n^V - \tilde{g}_n\|_{n,m} \leq \|g_0^V - \tilde{g}_n\|_{n,m} \leq \|g_0^V - g_0\|_{n,m} + \|g_0 - \tilde{g}_n\|_{n,m} \rightarrow \left\{ \int_{\mathbf{S}} (g_0(\mathbf{x}) - g_0^V(\mathbf{x}))^2 q(\mathbf{x}) d\mathbf{x} \right\}^{1/2}.$$

By comparing the above two equations (and taking ϵ to be sufficiently small), we conclude that as $n \rightarrow \infty$, with probability one,

$$\frac{1}{m} \sum_{i=1}^m \{\hat{g}_n^V(\mathbf{x}_i) - g_n^L(\mathbf{x}_i)\}^2 = \|\hat{g}_n^V - g_n^L\|_{2,\mathbf{S}}^2 \geq c$$

for some $c > 0$.

Finally, since $mT_{nk} = o_p(1)$ and $mT_n > c$ with probability one as $n \rightarrow \infty$, the consistency of the test can be shown using exactly the same argument shown in the final part of

the proof of Theorem 6. As such, we omit this part here for the sake of brevity.

□

D An algorithm for SCKLS computational performance

For a given number of evaluation points, m , SCKLS requires $m(m-1)$ concavity constraints. Larger values of m provide a more flexible functional estimate, but also increase the number of constraints quadratically, thus, the amount of time needed to solve the quadratic program also increases quadratically. Since one can select the number of evaluation points in SCKLS and CWB, by selecting m the computational complexity can be potentially reduced relative to CNLS or estimates on denser grids, i.e. with $m(m-1) \ll n(n-1)$.

Further, Dantzig et al. (1954, 1959) proposed an iterative approach that reduces the size of large-scale problems by relaxing a subset of the constraints and solving the relaxed model with only a subset V of constraints, checking which of the excluded constraints are violated, and iteratively adding violated constraints to the relaxed model until an optimal solution satisfies all constraints. Lee et al. (2013), who applied the approach to CNLS, found a significant reduction in computational time. Computational performances also improves if a subset of the constraints can be identified which are likely to be needed in the model. Lee et al. (2013) find the concavity constraints corresponding to pairs of observations that are close in terms of the ℓ_2 norm measured over input vectors and more likely to be binding than those corresponding to the distant observations. We use this insight to develop a strategy for identifying constraints to include in the initial subset V , when solving SCKLS as described below.

Given a grid to evaluate the constraints of the SCKLS estimator, we define the initial subset of constraints V as those constraints constructed by adjacent grid points as shown in Figure A.2. Further, we summarize our implementation of the algorithm proposed in Lee et al. (2013) below and label it as Algorithm 1.

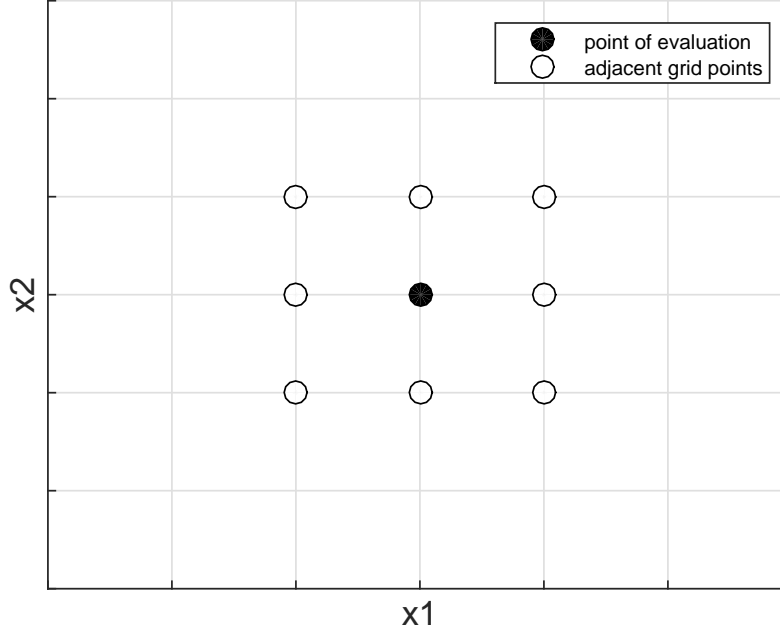


Figure A.2. Definition of adjacent grid in two-dimensional case.

Algorithm 1 Iterative approach for SCKLS computational speedup

```

 $t \leftarrow 0$ 
 $V \leftarrow \{(i, l) : \mathbf{x}_i \text{ and } \mathbf{x}_l \text{ are adjacent, } i < l\}$ 
Solve relaxed SCKLS with  $V$  to find initial solution  $\{a_i^{(0)}, \mathbf{b}_i^{(0)}\}_{i=1}^m$ 
while  $\{a_i^{(t)}, \mathbf{b}_i^{(t)}\}_{i=1}^m$  satisfies all constraints in (6) do
     $t \leftarrow t + 1$ 
     $U \leftarrow \{(i, l) : \mathbf{x}_i \text{ and } \mathbf{x}_l \text{ do not satisfy constraints in (6)}\}$ 
     $V \leftarrow V \cup U$ 
    Solve relaxed SCKLS with  $V$  to find solution  $\{a_i^{(t)}, \mathbf{b}_i^{(t)}\}_{i=1}^m$ 
end while
return  $\{a_i^{(t)}, \mathbf{b}_i^{(t)}\}_{i=1}^m$ 

```

E Comprehensive results of existing and additional numerical experiments

E.1 Uniform input – high signal-to-noise ratio (Experiment 1)

We compare the following seven estimators: SCKLS with fixed bandwidth, SCKLS with variable bandwidth, CNLS, CWB in p -space and CWB in y -space, Local Linear Kernel, and parametric Cobb-Douglas function estimated via ordinary least squares (OLS). Table A.4 and A.5 show the RMSE of Experiment 1 on observation points and evaluation points respectively.

Table A.6 shows the computational time of Experiment 1 for each estimator.

Table A.4. RMSE on observation points for Experiment 1

Number of observations		Average of RMSE on observation points				
		100	200	300	400	500
2-input	SCKLS fixed bandwidth	0.193	0.171	0.141	0.132	0.118
	SCKLS variable bandwidth	0.183	0.158	0.116	0.118	0.098
	CNLS	0.229	0.163	0.137	0.138	0.116
	CWB in p -space	0.189	0.167	0.158	0.140	0.129
	CWB in y -space	0.205	0.136	0.173	0.141	0.120
	Local Linear	0.212	0.166	0.149	0.152	0.140
Cobb-Douglas		0.078	0.075	0.048	0.039	0.043
3-input	SCKLS fixed bandwidth	0.230	0.187	0.183	0.152	0.165
	SCKLS variable bandwidth	0.216	0.183	0.175	0.143	0.142
	CNLS	0.294	0.202	0.189	0.173	0.168
	CWB in p -space	0.228	0.221	0.210	0.183	0.172
	CWB in y -space	0.209	0.362	0.218	0.154	0.160
	Local Linear	0.250	0.230	0.235	0.203	0.181
Cobb-Douglas		0.104	0.089	0.070	0.047	0.041
4-input	SCKLS fixed bandwidth	0.225	0.248	0.228	0.203	0.198
	SCKLS variable bandwidth	0.217	0.219	0.210	0.180	0.179
	CNLS	0.315	0.294	0.246	0.235	0.214
	CWB in p -space	0.238	0.262	0.231	0.234	0.198
	CWB in y -space	0.222	0.240	0.248	0.303	0.332
	Local Linear	0.256	0.297	0.252	0.240	0.226
Cobb-Douglas		0.120	0.073	0.091	0.067	0.063

Table A.5. RMSE on evaluation points for Experiment 1

Number of observations		Average of RMSE on evaluation points				
		100	200	300	400	500
2-input	SCKLS fixed bandwidth	0.219	0.189	0.150	0.147	0.128
	SCKLS variable bandwidth	0.212	0.176	0.125	0.132	0.103
	CNLS	0.350	0.299	0.260	0.284	0.265
	CWB in p -space	0.206	0.186	0.174	0.154	0.143
	CWB in y -space	0.259	0.228	0.228	0.172	0.167
	Local Linear	0.247	0.182	0.167	0.171	0.156
Cobb-Douglas		0.076	0.076	0.049	0.040	0.043
3-input	SCKLS fixed bandwidth	0.283	0.231	0.238	0.213	0.215
	SCKLS variable bandwidth	0.292	0.237	0.235	0.196	0.187
	CNLS	0.529	0.587	0.540	0.589	0.598
	CWB in p -space	0.291	0.289	0.269	0.252	0.233
	CWB in y -space	0.314	0.474	0.265	0.346	0.261
	Local Linear	0.336	0.340	0.360	0.326	0.264
Cobb-Douglas		0.116	0.098	0.080	0.052	0.046
4-input	SCKLS fixed bandwidth	0.321	0.357	0.329	0.308	0.290
	SCKLS variable bandwidth	0.378	0.348	0.363	0.320	0.301
	CNLS	0.845	0.873	0.901	0.827	0.792
	CWB in p -space	0.360	0.385	0.358	0.361	0.325
	CWB in y -space	0.355	0.470	0.338	0.410	0.602
	Local Linear	0.482	0.527	0.483	0.495	0.445
Cobb-Douglas		0.146	0.091	0.115	0.081	0.080

Table A.6. Computational time for Experiment 1

Number of observations		Average of computational time in seconds; (percentage of Afriat constraints included in the final optimization problem)				
		100	200	300	400	500
2-input	SCKLS fixed bandwidth	14.1 (6.14%)	13.3 (5.28%)	42.2 (8.86%)	34.7 (7.80%)	77.4 (8.31%)
	SCKLS variable bandwidth	16.4 (3.47%)	33.9 (3.44%)	27.6 (3.34%)	36.0 (3.22%)	50.6 (3.53%)
	CNLS	2.0 (100%)	6.1 (100%)	16.5 (100%)	26.5 (100%)	55.3 (100%)
	CWB in p -space	24.1 (2.39%)	33.2 (2.35%)	76.6 (2.35%)	82.3 (2.35%)	130 (2.35%)
	CWB in y -space	39.3 (2.35%)	92.7 (2.35%)	111 (2.35%)	190 (2.35%)	233 (2.36%)
3-input	SCKLS fixed bandwidth	26.9 (16.0%)	40.4 (16.6%)	45.5 (16.3%)	67.3 (16.4%)	136 (16.2%)
	SCKLS variable bandwidth	20.0 (15.7%)	42.0 (15.9%)	37.4 (15.8%)	47.1 (15.8%)	58.2 (15.9%)
	CNLS	3.8 (100%)	16.4 (100%)	37.0 (100%)	82.9 (100%)	161 (100%)
	CWB in p -space	47.6 (15.5%)	71.5 (15.5%)	100 (15.5%)	202 (15.5%)	255 (15.5%)
	CWB in y -space	120 (15.5%)	357 (15.5%)	443 (15.5%)	529 (15.5%)	424 (15.5%)
4-input	SCKLS fixed bandwidth	47.5 (40.1%)	71.6 (39.9%)	77.4 (39.9%)	166 (40.0%)	235 (39.8%)
	SCKLS variable bandwidth	26.8 (39.9%)	45.6 (40.0%)	46.8 (39.8%)	60.5 (39.9%)	74.8 (39.8%)
	CNLS	5.8 (100%)	22.4 (100%)	79.1 (100%)	139.8 (100%)	287.8 (100%)
	CWB in p -space	68.8 (39.8%)	136 (39.8%)	196 (39.8%)	327 (39.8%)	442 (39.8%)
	CWB in y -space	91.3 (39.8%)	175 (39.8%)	195 (39.8%)	535 (39.8%)	545 (39.8%)

E.2 Uniform input – low signal-to-noise ratio (Experiment 2)

We compare following seven estimators: SCKLS with fixed bandwidth, SCKLS with variable bandwidth, CNLS, CWB in p -space, CWB in y -space, Local Linear Kernel, and parametric Cobb-Douglas function estimated via ordinary least squares (OLS). Table A.7 and A.8 show the RMSE of Experiment 2 on observation points and evaluation points respectively.

Table A.7. RMSE on observation points for Experiment 2

Number of observations		Average of RMSE on observation points				
		100	200	300	400	500
2-input	SCKLS fixed bandwidth	0.239	0.203	0.203	0.155	0.140
	SCKLS variable bandwidth	0.240	0.185	0.168	0.139	0.119
	CNLS	0.279	0.231	0.194	0.168	0.151
	CWB in p -space	0.314	0.215	0.237	0.275	0.151
	CWB in y -space	0.241	0.229	0.173	0.178	0.206
	Local Linear	0.287	0.244	0.230	0.214	0.161
	Cobb-Douglas	0.109	0.108	0.081	0.042	0.048
3-input	SCKLS fixed bandwidth	0.292	0.263	0.221	0.204	0.184
	SCKLS variable bandwidth	0.281	0.242	0.198	0.180	0.175
	CNLS	0.379	0.303	0.275	0.224	0.214
	CWB in p -space	0.318	0.306	0.308	0.244	0.214
	CWB in y -space	0.281	0.273	0.225	0.320	0.271
	Local Linear	0.333	0.306	0.288	0.259	0.214
	Cobb-Douglas	0.176	0.118	0.101	0.084	0.072
4-input	SCKLS fixed bandwidth	0.317	0.291	0.249	0.241	0.254
	SCKLS variable bandwidth	0.290	0.254	0.236	0.222	0.215
	CNLS	0.491	0.356	0.311	0.293	0.313
	CWB in p -space	0.400	0.318	0.273	0.260	0.289
	CWB in y -space	0.312	0.338	0.262	0.365	0.453
	Local Linear	0.335	0.342	0.257	0.274	0.283
	Cobb-Douglas	0.157	0.150	0.112	0.075	0.077

Table A.8. RMSE on evaluation points for Experiment 2

Number of observations		Average of RMSE on evaluation points				
		100	200	300	400	500
2-input	SCKLS fixed bandwidth	0.253	0.225	0.222	0.172	0.160
	SCKLS variable bandwidth	0.255	0.205	0.179	0.149	0.135
	CNLS	0.319	0.355	0.334	0.255	0.267
	CWB in p -space	0.329	0.239	0.262	0.305	0.177
	CWB in y -space	0.263	0.241	0.198	0.228	0.180
	Local Linear	0.330	0.272	0.257	0.239	0.194
	Cobb-Douglas	0.112	0.112	0.083	0.044	0.049
3-input	SCKLS fixed bandwidth	0.367	0.339	0.302	0.268	0.231
	SCKLS variable bandwidth	0.364	0.303	0.256	0.230	0.224
	CNLS	0.743	0.778	0.744	0.696	0.620
	CWB in p -space	0.398	0.392	0.434	0.336	0.274
	CWB in y -space	0.401	0.473	0.385	0.450	0.525
	Local Linear	0.452	0.444	0.438	0.398	0.302
	Cobb-Douglas	0.202	0.130	0.110	0.093	0.079
4-input	SCKLS fixed bandwidth	0.405	0.460	0.349	0.350	0.347
	SCKLS variable bandwidth	0.419	0.434	0.375	0.354	0.315
	CNLS	1.019	0.950	0.985	1.043	1.106
	CWB in p -space	0.514	0.520	0.393	0.390	0.452
	CWB in y -space	0.514	0.513	0.425	0.501	0.708
	Local Linear	0.524	0.626	0.451	0.491	0.550
	Cobb-Douglas	0.187	0.194	0.134	0.092	0.091

E.3 Non-uniform input (Experiment 3)

We compare following seven estimators: SCKLS with fixed bandwidth with uniform/non-uniform grid, SCKLS with variable bandwidth with uniform/non-uniform grid, CNLS, CWB in p -space with uniform/non-uniform grid. Table A.9 and A.10 show the RMSE of Experiment 3 on observation points and evaluation points respectively.

Table A.9. RMSE on observation points for Experiment 3

Number of observations		Average of RMSE on observation points				
		100	200	300	400	500
2-input	SCKLS fixed/uniform	0.179	0.151	0.144	0.121	0.108
	SCKLS fixed/non-uniform	0.185	0.153	0.159	0.123	0.107
	SCKLS variable/uniform	0.183	0.156	0.142	0.125	0.104
	SCKLS variable/non-uniform	0.176	0.144	0.132	0.114	0.093
	CNLS	0.193	0.160	0.140	0.130	0.117
	CWB p -space/uniform	0.256	0.162	0.180	0.139	0.125
	CWB p -space/non-uniform	0.243	0.160	0.174	0.135	0.125
3-input	SCKLS fixed/uniform	0.197	0.184	0.172	0.164	0.167
	SCKLS fixed/non-uniform	0.200	0.181	0.173	0.161	0.172
	SCKLS variable/uniform	0.212	0.187	0.170	0.175	0.170
	SCKLS variable/non-uniform	0.210	0.180	0.162	0.160	0.155
	CNLS	0.303	0.246	0.201	0.185	0.166
	CWB p -space/uniform	0.243	0.436	0.173	0.174	0.184
	CWB p -space/non-uniform	0.233	0.194	0.176	0.165	0.173
4-input	SCKLS fixed/uniform	0.219	0.211	0.196	0.209	0.187
	SCKLS fixed/non-uniform	0.210	0.206	0.181	0.197	0.180
	SCKLS variable/uniform	0.208	0.193	0.167	0.171	0.170
	SCKLS variable/non-uniform	0.206	0.193	0.164	0.169	0.168
	CNLS	0.347	0.292	0.250	0.228	0.218
	CWB p -space/uniform	0.219	0.205	0.205	0.184	0.218
	CWB p -space/non-uniform	0.221	0.205	0.182	0.170	0.170

Table A.10. RMSE on evaluation points for Experiment 3

Number of observations		Average of RMSE on evaluation points				
		100	200	300	400	500
2-input	SCKLS fixed/uniform	0.262	0.220	0.244	0.157	0.196
	SCKLS fixed/non-uniform	0.212	0.174	0.195	0.138	0.131
	SCKLS variable/uniform	0.246	0.204	0.192	0.142	0.136
	SCKLS variable/non-uniform	0.193	0.160	0.145	0.120	0.100
	CNLS	0.435	0.402	0.404	0.379	0.381
	CWB p -space/uniform	0.422	0.287	0.376	0.246	0.264
	CWB p -space/non-uniform	0.283	0.186	0.215	0.159	0.162
3-input	SCKLS fixed/uniform	0.323	0.308	0.311	0.286	0.293
	SCKLS fixed/non-uniform	0.268	0.254	0.259	0.235	0.249
	SCKLS variable/uniform	0.335	0.303	0.281	0.262	0.254
	SCKLS variable/non-uniform	0.278	0.243	0.219	0.212	0.196
	CNLS	0.828	0.824	0.828	0.786	0.782
	CWB p -space/uniform	0.438	0.684	0.357	0.363	0.350
	CWB p -space/non-uniform	0.315	0.265	0.257	0.235	0.242
4-input	SCKLS fixed/uniform	0.406	0.398	0.397	0.404	0.400
	SCKLS fixed/non-uniform	0.339	0.343	0.333	0.371	0.331
	SCKLS variable/uniform	0.417	0.423	0.368	0.364	0.356
	SCKLS variable/non-uniform	0.359	0.359	0.313	0.302	0.280
	CNLS	1.129	1.107	1.220	1.196	1.223
	CWB p -space/uniform	0.421	0.442	0.435	0.418	0.487
	CWB p -space/non-uniform	0.354	0.344	0.308	0.286	0.280

E.4 Different numbers of evaluation points (Experiment 4)

We compare following four estimators: SCKLS with fixed bandwidth, SCKLS with variable bandwidth, CWB in p -space and CWB in y -space. Table A.11 and A.12 show the RMSE of Experiment 4 on observation points and evaluation points respectively. In addition, Table A.13 shows the computational time of Experiment 4 for each estimator.

Table A.11. RMSE on observation points for Experiment 4

Number of evaluation points		Average of RMSE on observation points		
		100	300	500
2-input	SCKLS fixed bandwidth	0.142	0.141	0.141
	SCKLS variable bandwidth	0.113	0.112	0.112
	CWB in p -space	0.149	0.151	0.156
	CWB in y -space	0.225	0.122	0.129
3-input	SCKLS fixed bandwidth	0.198	0.203	0.197
	SCKLS variable bandwidth	0.169	0.167	0.166
	CWB in p -space	0.218	0.234	0.231
	CWB in y -space	0.345	0.241	0.222
4-input	SCKLS fixed bandwidth	0.239	0.207	0.206
	SCKLS variable bandwidth	0.195	0.192	0.191
	CWB in p -space	0.219	0.227	0.296
	CWB in y -space	0.466	0.290	0.292

Table A.12. RMSE on evaluation points for Experiment 4

Number of evaluation points		Average of RMSE on evaluation points		
		100	300	500
2-input	SCKLS fixed bandwidth	0.181	0.164	0.158
	SCKLS variable bandwidth	0.140	0.128	0.124
	CWB in p -space	0.195	0.180	0.179
	CWB in y -space	0.262	0.162	0.169
3-input	SCKLS fixed bandwidth	0.304	0.267	0.257
	SCKLS variable bandwidth	0.242	0.213	0.205
	CWB in p -space	0.332	0.329	0.302
	CWB in y -space	0.792	0.582	0.559
4-input	SCKLS fixed bandwidth	0.383	0.296	0.270
	SCKLS variable bandwidth	0.386	0.304	0.265
	CWB in p -space	0.403	0.359	0.415
	CWB in y -space	1.040	0.352	0.381

Table A.13. Computational time for Experiment 4

Number of evaluation points		Average of computational time in seconds; (percentage of Afriat constraints included in the final optimization)		
		100	300	500
2-input	SCKLS fixed bandwidth	26.6 (11.7%)	28.3 (6.6%)	34 (5.4%)
	SCKLS variable bandwidth	21.3 (9.9%)	21.6 (4.4%)	24.9 (3.2%)
	CWB in p -space	41 (8.8%)	56.5 (3.2%)	74.2 (2.0%)
	CWB in y -space	52.8 (8.8%)	103 (3.2%)	146 (2.0%)
3-input	SCKLS fixed bandwidth	84.8 (29.1%)	112 (16.7%)	134 (13.3%)
	SCKLS variable bandwidth	21.1 (28.5%)	37.2 (15.8%)	59.1 (12.4%)
	CWB in p -space	121 (28.2%)	221 (15.5%)	310 (12.2%)
	CWB in y -space	181 (28.2%)	625 (15.5%)	948 (12.2%)
4-input	SCKLS fixed bandwidth	149 (62.3%)	170 (40.0%)	597 (27.7%)
	SCKLS variable bandwidth	24.6 (62.1%)	52.7 (39.9%)	468 (27.5%)
	CWB in p -space	175 (61.9%)	275 (39.8%)	729 (27.4%)
	CWB in y -space	189 (61.9%)	288 (39.8%)	579 (27.4%)

E.5 Estimation with a misspecified shape (additional experiment)

Experiment 8. We use the DGP proposed by Olesen and Ruggiero (2014) that is consistent with the regular ultra passum law (Frisch, 1964), which appears to have an “S”-shape.

$$g_0(x_1, x_2) = F(h(x_1, x_2))$$

where the scaling function is: $F(w) = \frac{15}{1+e^{-5\log(w)}}$, and the linear homogeneous core function is: $h(x_1, x_2) = \left(\beta x_1^{\frac{\sigma-1}{\sigma}} + (1-\beta)x_2^{\frac{\sigma-1}{\sigma}} \right)^{\frac{\sigma}{\sigma-1}}$ with $\beta = 0.45$ and $\sigma = 1.51$. For $j = 1, \dots, n$, input, $\mathbf{X}_j = (x_{j1}, x_{j2})^T$, is generated in polar coordinates with angles η and modulus ω independently uniformly distributed on $[0.05, \pi/2 - 0.05]$ and $[0, 2.5]$, respectively. The additive noise, ϵ_j , is randomly sampled from $N(0, 0.7^2)$.

Note that this DGP is not concave. Here we run this experiment to assess the performance of each estimator in case of shape misspecification. Table A.14 and A.15 show the RMSE of this experiment on observation points and evaluation points. The SCKLS estimator is competitive to the CNLS estimator on observation points where the CNLS estimator has certain convergence properties even for the misspecified functional form (See Lim and Glynn (2012) for details). Consistency for the misspecified functional form indicates that the estimator converges to the closest shape constrained functional estimate in the violated area. In case of this experiment, the CNLS estimator converges to closest concave/monotonic function in the violated area (convex), which is linear function. Since the SCKLS estimator is competitive to the CNLS estimator, we could empirically show that the SCKLS estimator also has consistency for the misspecified functional form. Thus, the SCKLS estimator has relatively robust performance even with data generated by the misspecified functional form. Figure A.3 shows the estimation results with 1-input S-shape function from a typical run. The figure shows that the SCKLS estimator results in a linear estimates for areas where concavity is violated. Here the CWB estimator performs poorly when the function is misspecified although it has consistency properties shown by Du et al. (2013). The main reason for this is that the optimization problem becomes too complicated to solve since intuitively there are many binding constraints when the data is generated by the misspecified functional form, and thus, it becomes hard for the solver to find a feasible

solution and an improving direction.

Table A.14. RMSE on observation points for Experiment 8

Number of observations	Average of RMSE on observation points				
	100	200	300	400	500
SCKLS fixed bandwidth	1.424	1.435	1.405	1.392	1.421
CNLS	1.326	1.346	1.337	1.316	1.353
CWB in p-space	6.310	6.731	6.602	5.909	6.110

Table A.15. RMSE on evaluation points for Experiment 8

Number of observations	Average of RMSE on evaluation points				
	100	200	300	400	500
SCKLS fixed bandwidth	1.337	1.162	1.149	1.140	1.123
CNLS	1.375	1.424	1.404	1.403	1.385
CWB in p-space	9.100	9.483	9.599	8.435	8.719

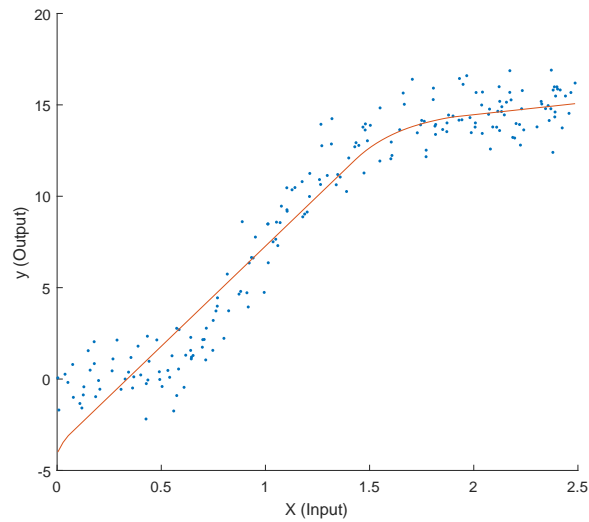


Figure A.3. Applying the SCKLS estimator to the S-shape function.

E.6 Test against monotonicity and concavity (Experiment 6)

We show the comprehensive results of Experiment 6. Table A.16 show the rejection rate of the test for monotonicity and concavity, where different sample sizes $n = 100, 300, 500$ and the number of inputs $d = 1, 2, 3$ are considered.

Table A.16. Rejection rate of test for monotonicity and concavity

Sample size (n)	Shape Parameter (p)	Power of the Test (α)								
		$d = 1$			$d = 2$			$d = 3$		
		0.10	0.05	0.01	0.10	0.05	0.01	0.10	0.05	0.01
100	0.2	0.00	0.00	0.00	0.02	0.00	0.00	0.37	0.28	0.13
	0.5	0.00	0.00	0.00	0.01	0.01	0.00	0.35	0.20	0.08
	1.0	0.03	0.00	0.00	0.08	0.05	0.01	0.49	0.38	0.11
	2.0	1.00	1.00	1.00	0.98	0.93	0.82	0.98	0.95	0.77
	5.0	1.00	1.00	1.00	1.00	1.00	1.00	1.00	1.00	1.00
	S-shape	1.00	1.00	0.97	0.73	0.64	0.42	0.80	0.71	0.45
300	0.2	0.00	0.00	0.00	0.00	0.00	0.00	0.05	0.02	0.01
	0.5	0.00	0.00	0.00	0.00	0.00	0.00	0.03	0.01	0.00
	1.0	0.02	0.00	0.00	0.03	0.03	0.00	0.37	0.25	0.08
	2.0	1.00	1.00	1.00	1.00	1.00	1.00	1.00	1.00	0.95
	5.0	1.00	1.00	1.00	1.00	1.00	1.00	1.00	1.00	1.00
	S-shape	1.00	1.00	1.00	0.99	0.99	0.98	0.93	0.88	0.78
500	0.2	0.00	0.00	0.00	0.00	0.00	0.00	0.02	0.02	0.01
	0.5	0.00	0.00	0.00	0.00	0.00	0.00	0.03	0.02	0.01
	1.0	0.00	0.00	0.00	0.01	0.01	0.00	0.17	0.10	0.02
	2.0	1.00	1.00	1.00	1.00	1.00	1.00	1.00	1.00	0.97
	5.0	1.00	1.00	1.00	1.00	1.00	1.00	1.00	1.00	1.00
	S-shape	1.00	1.00	1.00	1.00	1.00	1.00	0.99	0.96	0.85

F Semiparametric partially linear model

We develop a semiparametric partially linear model including the SCKLS estimator and a linear function of contextual variables. The partially linear model is often used in practice. The model estimated is represented as follows:

$$y_j = \mathbf{Z}_j' \boldsymbol{\gamma} + g_0(\mathbf{X}_j) + \epsilon_j$$

where $\mathbf{Z}_j = (Z_{j1}, Z_{j2}, \dots, Z_{jl})'$ denotes contextual variables and $\boldsymbol{\gamma} = (\gamma_1, \gamma_2, \dots, \gamma_l)'$ is the coefficient of contextual variables, see Johnson and Kuosmanen (2011, 2012). Then, we estimate the coefficient of contextual variable:

$$\hat{\boldsymbol{\gamma}} = \left(\sum_{j=1}^n \tilde{\mathbf{Z}}_j \tilde{\mathbf{Z}}_j' \right)^{-1} \left(\sum_{j=1}^n \tilde{\mathbf{Z}}_j \tilde{y}_j \right)$$

where $\tilde{\mathbf{Z}}_j = \mathbf{Z}_j - \hat{E}[\mathbf{Z}_j | \mathbf{X}_j]$ and $\tilde{y}_j = y_j - \hat{E}[y_j | \mathbf{X}_j]$ respectively, and each conditional expectation is estimated by kernel estimation method such as local linear. Finally, we apply the SCKLS estimator to the data $\{\mathbf{X}_j, y_j - \mathbf{Z}_j' \hat{\boldsymbol{\gamma}}\}_{j=1}^n$. Robinson (1988) proved that $\hat{\boldsymbol{\gamma}}$ is $n^{1/2}$ -consistent for $\boldsymbol{\gamma}$ and asymptotically normal under regularity conditions. For details of the partially linear model, see Li and Racine (2007).

We conduct an experiment to compare the performance of SCKLS and CNLS estimator with contextual variables.

Experiment 9. We use DGPs from Experiment 1. We consider the model with Cobb–Douglas function with contextual variables.

$$g_0(\mathbf{x}, z) = \prod_{k=1}^d x_k^{\frac{0.8}{d}} + z\gamma, \tag{A.4}$$

where for each (\mathbf{X}_j, Z_j, y_j) , the contextual variable Z_j is a scalar value independent of \mathbf{X}_j drawn randomly and independently from $unif[0, 1]$, the coefficient of the contextual variable $\gamma = 5$, and other parameters follow DGP from Experiment 1. We compare the performance of SCKLS with and without contextual variables by comparing estimators with the true production function.

Table A.17 and A.18 show the RMSE of this experiment on observation points and evaluation points respectively. The RMSE is obtained by comparing estimates of production function and the true production function. Here, the production function is indicated by the first term of the right hand-side of Equation (A.4). The SCKLS estimator with Z -variable is competitive to the SCKLS estimator without Z -variable when dimension of input is small. Furthermore, when the number of observations increases, the SCKLS estimator with Z -variable performs better than the SCKLS without Z -variable. These findings are consistent with the work of Robinson (1988). Since our application data in Section 7 has only two-input, we could empirically show that the SCKLS with Z -variable does not deteriorate the estimate performance of the production function in our application.

Table A.17. RMSE on observation points for experiments with/without Z -variable

Number of observations		Average of RMSE on observation points				
		100	200	300	400	500
2-input	SCKLS-Z	0.224	0.212	0.239	0.160	0.146
	SCKLS	0.210	0.188	0.170	0.139	0.140
3-input	SCKLS-Z	0.404	0.235	0.261	0.197	0.196
	SCKLS	0.242	0.206	0.215	0.202	0.188
4-input	SCKLS-Z	0.462	0.376	0.332	0.217	0.239
	SCKLS	0.247	0.231	0.202	0.202	0.198

Table A.18. RMSE on evaluation points for experiments with/without Z -variable

Number of observations		Average of RMSE on evaluation points				
		100	200	300	400	500
2-input	SCKLS-Z	0.245	0.234	0.256	0.172	0.166
	SCKLS	0.230	0.205	0.194	0.154	0.157
3-input	SCKLS-Z	0.496	0.348	0.377	0.271	0.286
	SCKLS	0.316	0.296	0.309	0.271	0.261
4-input	SCKLS-Z	0.648	0.599	0.498	0.397	0.435
	SCKLS	0.385	0.381	0.341	0.350	0.336

References

- Ackerberg, D. A., K. Caves, and G. Frazer (2015). Identification properties of recent production function estimators. *Econometrica* 83(6), 2411–2451.
- Afriat, S. N. (1972). Efficiency estimation of production functions. *International Economic Review* 13(3), 568–598.
- Alvarez, R. and H. Görg (2009). Multinationals and plant exit: Evidence from chile. *International Review of Economics & Finance* 18(1), 45–51.
- Alvarez, R. and R. Robertson (2004). Exposure to foreign markets and plant-level innovation: evidence from chile and mexico. *The Journal of International Trade & Economic Development* 13(1), 57–87.
- Banker, R. D. and A. Maindiratta (1992). Maximum likelihood estimation of monotone and concave production frontiers. *Journal of Productivity Analysis* 3(4), 401–415.
- Benavente, J. M. (2006). The role of research and innovation in promoting productivity in chile. *Economics of Innovation and New Technology* 15(4-5), 301–315.
- Benavente, J. M. and C. Ferrada (2003). Probability of survival of new manufacturing plants: the case of chile.. *Unpublished manuscript, Universidad de Chile*.
- Beresteanu, A. (2005). Nonparametric analysis of cost complementarities in the telecommunications industry. *RAND Journal of Economics* 36(4), 870–889.
- Bernard, A. B. and J. B. Jensen (2004). Exporting and productivity in the usa. *Oxford Review of Economic Policy* 20(3), 343–357.
- Bertsekas, D. (1995). *Nonlinear Programming*. Athena Scientific.
- Birke, M. and H. Dette (2007). Estimating a convex function in nonparametric regression. *Scandinavian Journal of Statistics* 34(2), 384–404.
- Brunk, H. D. (1955). Maximum likelihood estimates of monotone parameters. *The Annals of Mathematical Statistics* 26(4), 607–616.

- Carroll, R. J., A. Delaigle, and P. Hall (2011). Testing and estimating shape-constrained nonparametric density and regression in the presence of measurement error. *Journal of the American Statistical Association* 106(493), 191–202.
- Chen, X. and Y. J. Qiu (2016). Methods for nonparametric and semiparametric regressions with endogeneity: a gentle guide. Cowles Foundation Discussion Papers 2032, Cowles Foundation for Research in Economics, Yale University.
- Chen, Y. and J. A. Wellner (2016). On convex least squares estimation when the truth is linear. *Electronic Journal of Statistics* 10(1), 171–209.
- Cleveland, W. S. (1979). Robust locally weighted regression and smoothing scatterplots. *Journal of the American statistical association* 74(368), 829–836.
- Dantzig, G., R. Fulkerson, and S. Johnson (1954). Solution of a large-scale traveling-salesman problem. *Journal of the operations research society of America* 2(4), 393–410.
- Dantzig, G. B., D. R. Fulkerson, and S. M. Johnson (1959). On a linear-programming, combinatorial approach to the traveling-salesman problem. *Operations Research* 7(1), 58–66.
- De Loecker, J. (2007). Do exports generate higher productivity? evidence from slovenia. *Journal of international economics* 73(1), 69–98.
- Diewert, W. and T. J. Wales (1987). Flexible functional forms and global curvature conditions. *Econometrica* 55(1), 43–68.
- DiNardo, J. and J. L. Tobias (2001). Nonparametric density and regression estimation. *The Journal of Economic Perspectives* 15(4), 11–28.
- Du, P., C. F. Parmeter, and J. S. Racine (2013). Nonparametric kernel regression with multiple predictors and multiple shape constraints. *Statistica Sinica* 23(3), 1347–1371.
- Fan, Y. and E. Guerre (2016). Multivariate local polynomial estimators: Uniform boundary properties and asymptotic linear representation. In *Essays in Honor of Aman Ullah*, pp. 489–537. Emerald.

- Frisch, R. (1964). *Theory of production*. Springer.
- Ghosal, P. and B. Sen (2016). On univariate convex regression. *arXiv preprint arXiv:1608.04167*.
- Grenander, U. (1956). On the theory of mortality measurement: part ii. *Scandinavian Actuarial Journal* 1956(2), 125–153.
- Grenander, U. (1981). *Abstract Inference*. John Wiley & Sons.
- Groeneboom, P., G. Jongbloed, and J. A. Wellner (2001). Estimation of a convex function: characterizations and asymptotic theory. *The Annals of Statistics* 29(6), 1653–1698.
- Hall, P. and L.-S. Huang (2001). Nonparametric kernel regression subject to monotonicity constraints. *The Annals of Statistics* 29(3), 624–647.
- Hanson, D. and G. Pledger (1976). Consistency in concave regression. *The Annals of Statistics* 4(6), 1038–1050.
- Hildreth, C. (1954). Point estimates of ordinates of concave functions. *Journal of the American Statistical Association* 49(267), 598–619.
- Johnson, A. L. and T. Kuosmanen (2011). One-stage estimation of the effects of operational conditions and practices on productive performance: asymptotically normal and efficient, root-n consistent stonezd method. *Journal of productivity analysis* 36(2), 219–230.
- Johnson, A. L. and T. Kuosmanen (2012). One-stage and two-stage dea estimation of the effects of contextual variables. *European Journal of Operational Research* 220(2), 559–570.
- Kuosmanen, T. (2008). Representation theorem for convex nonparametric least squares. *The Econometrics Journal* 11(2), 308–325.
- Kuosmanen, T. and M. Kortelainen (2012). Stochastic non-smooth envelopment of data: semi-parametric frontier estimation subject to shape constraints. *Journal of Productivity Analysis* 38(1), 11–28.

- Lee, C.-Y., A. L. Johnson, E. Moreno-Centeno, and T. Kuosmanen (2013). A more efficient algorithm for convex nonparametric least squares. *European Journal of Operational Research* 227(2), 391–400.
- Li, Q. and J. S. Racine (2007). *Nonparametric econometrics: theory and practice*. Princeton University Press.
- Li, Z., G. Liu, and Q. Li (2016). Nonparametric knn estimation with monotone constraints. Working paper.
- Lim, E. and P. W. Glynn (2012). Consistency of multidimensional convex regression. *Operations Research* 60(1), 196–208.
- Mammen, E. (1991). Nonparametric regression under qualitative smoothness assumptions. *The Annals of Statistics* 19(2), 741–759.
- Marschak, J. and W. H. Andrews (1944). Random simultaneous equations and the theory of production. *Econometrica* 12(3/4), 143–205.
- Masry, E. (1996). Multivariate local polynomial regression for time series: Uniform strong consistency and rates. *Journal of Time Series Analysis* 17(6), 571–599.
- Mazumder, R., A. Choudhury, G. Iyengar, and B. Sen (2015). A Computational Framework for Multivariate Convex Regression and its Variants. *arXiv preprint arXiv:1509.08165*.
- Nemoto, J. and M. Goto (2004). Technological externalities and economies of vertical integration in the electric utility industry. *International Journal of Industrial Organization* 22(1), 67–81.
- Nesterov, Y. (2005). Smooth minimization of non-smooth functions. *Mathematical programming* 103(1), 127–152.
- Olesen, O. B. and J. Ruggiero (2014). Maintaining the regular ultra passum law in data envelopment analysis. *European Journal of Operational Research* 235(3), 798–809.
- Pavcnik, N. (2002). Trade liberalization, exit, and productivity improvements: Evidence from chilean plants. *The Review of Economic Studies* 69(1), 245–276.

- Racine, J. and Q. Li (2004). Nonparametric estimation of regression functions with both categorical and continuous data. *Journal of Econometrics* 119(1), 99–130.
- Racine, J. S. (2016). Local polynomial derivative estimation: Analytic or Taylor? In *Essays in Honor of Aman Ullah*, pp. 617–633. Emerald.
- Robinson, P. M. (1988). Root-n-consistent semiparametric regression. *Econometrica* 56(4), 931–954.
- Rockafellar, R. T. (1970). *Convex Analysis*. Princeton University Press.
- Sarath, B. and A. Maindiratta (1997). On the consistency of maximum likelihood estimation of monotone and concave production frontiers. *Journal of Productivity Analysis* 8(3), 239–246.
- Seijo, E. and B. Sen (2011). Nonparametric least squares estimation of a multivariate convex regression function. *The Annals of Statistics* 39(3), 1633–1657.
- Sen, B. and M. Meyer (2017). Testing against a linear regression model using ideas from shape-restricted estimation. *Journal of the Royal Statistical Society: Series B (Statistical Methodology)* 2(79), 423–448.
- Stone, C. J. (1977). Consistent nonparametric regression. *The Annals of Statistics* 5(4), 595–620.
- van der Vaart, A. and J. Wellner (1996). *Weak Convergence and Empirical Processes: With Applications to Statistics*. Springer Series in Statistics. Springer.
- Varian, H. R. (1982). The nonparametric approach to demand analysis. *Econometrica* 50(4), 945–973.
- Varian, H. R. (1984). The nonparametric approach to production analysis. *Econometrica* 52(3), 579–597.